Characteristics of GABAergic and Cholinergic Neurons in the Perinuclear Zone of Mouse Supraoptic Nucleus

Lie Wang[1], Matthew Ennis[1], Gábor Szabó[2] and William E. Armstrong[1]

[1]Department of Anatomy and Neurobiology and Neuroscience Institute

University of Tennessee Health Science Center

Memphis, TN 38163

[2] Department of Gene Technology and Developmental Biology

Institute of Experimental Medicine

1083 Budapest, Hungary

Running title: Cholinergic and GABAergic Supraoptic Perinuclear Neurons

Key words: interneurons, GABA, acetylcholine, oxytocin, vasopressin

Total number of words: 7,313

Figures: 10

Tables: 0

Correspondence:

Lie Wang, M.D.

Department of Anatomy and Neurobiology

University of Tennessee Health Science Center

Memphis, TN, USA 38163

Phone: 901-448-5995

Fax: 901-448-7193

Email: lwang5@uthsc.edu

Abstract

The perinuclear zone (PNZ) of the supraoptic nucleus (SON) contains some GABAergic and cholinergic neurons thought to innervate the SON proper. In transgenic mice expressing enhanced Green Fluorescent Protein (eGFP) in association with glutamate decarboxylase (GAD), 65, we found an abundance of GAD65-eGFP neurons in the PNZ. In contrast, in another strain expressing GAD67-eGFP, there were few labeled PNZ neurons. In a third mouse line expressing choline acetyltransferase (ChAT)-eGFP, large, brightly fluorescent and small, dimly fluorescent ChAT-eGFP neurons were present in the PNZ. Virtually all small neurons (GAD65-positive, or ChAT-positive), exhibited a low threshold depolarizing potential consistent with a low threshold spike (LTS) and exhibited little transient outward rectification. Many of these neurons fired spontaneously. In contrast, large ChAT-eGFP neurons exhibited strong transient outward rectification consistent with an A-type current, were electrically silent, and possessed a large hyperpolarizing spike afterpotential. Large ChAT-eGFP neurons were immunostained with ChAT antibody (AB144p), whereas the smaller ChAT-eGFP neurons were not. Reconstructed neurons revealed a few processes encroaching near and passing through the SON from all types, but no clear evidence of a terminal axon arbor. Large ChAT-eGFP neurons were usually oriented vertically, had 4-5 dendrites with a varicose appearance and multiple branches, and most had an axon with many collaterals and local arborizations. Small ChAT-eGFP neurons in the PNZ had a much more restricted dendritic tree compared to parvocellular GAD65 neurons, the latter of which had long thin processes oriented medio-laterally. Thus many of the characteristics found in unidentified, small PNZ neurons in a previous study are also found in identified GABAergic neurons, and in a population of smaller ChAT-eGFP neurons, whose cholinergic identity must be further verified. The large soma and prominent transient outward rectification of large ChAT-eGFP neurons suggests these features are insufficient to distinguish them from magnocellular SON neurons in dissociated preparations, or in blind recordings that might involve the PNZ.

Introduction

Unlike many areas of the central nervous system, the rodent supraoptic nucleus (SON) of the hypothalamus does not possess a well-characterized population of interneurons. Most SON neurons are considered magnocellular neurosecretory cells (MNCs; ≥ 20 μm soma diameter), synthesize oxytocin (OT) or vasopressin (VP), possess 1-3 sparsely branching dendrites and project an axon to the neurohypophysis where these hormones are released near fenestrated capillaries for systemic distribution (Armstrong, 1995; 2014). In Golgi studies of rat, Bruni and Perumal (1984) and Dyball and Kemply (1983) described a few smaller neurons in the SON with a different morphology, and similar neurons have been observed in rabbit (Felten and Casher, 1979) and monkey (LuQui and Fox, 1976). Iijima and Saito (1983) also described small group of neurons that stained histochemically for GABA transaminase, unlike the MNCs.

In contrast to the paucity of evidence for classic interneurons within the SON, investigators have suggested that the perinuclear zone (PNZ) immediately dorsal to the SON contains neurons that project to the SON and could functionally serve as interneurons. Small tracer injections into the SON retrogradely label PNZ neurons (Iijima and Ogawa, 1981; Jhamandas et al., 1989; Raby and Renaud, 1989; Tribollet et al., 1985), and transneuronal transport of pseudorabies virus following neurohypophysial injections has been observed in the PNZ (Levine et al., 1994). Complementarily, anterograde transport of the plant lectin *Phaseolous vulgaris leucoagglutinin*, from the PNZ to the SON has been reported (Roland and Sawchenko, 1993). Neurons in this region could account for the large number of intact synapses remaining in the SON after its surgical isolation (Léranth et al., 1975). The PNZ contains GABAergic neurons (Tappaz et al., 1983; Theodosis et al., 1986) that are thought to mediate the rapid inhibition of VP neurons following transient hypertension (Jhamandas et al., 1989; Nissen et al., 1993). Although

anatomical evidence is lacking, glutamatergic PNZ neurons also have been postulated since local stimulation of these region can produced inhibitory or excitatory postsynaptic potentials in SON neurons (Boudaba et al., 1997; Wuarin, 1997). Finally, a group of cholinergic neurons was identified in the PNZ with processes projecting into the SON (Mason et al., 1983). While these were later described as dendrites rather than synapse-forming axons (Meeker et al., 1988; Theodosis and Mason, 1988), stimulation of the PNZ does evoke monosynaptic excitatory synaptic potentials in the SON blocked by selective nicotinic receptor antagonists, and inhibition of acetylcholinesterase activity increases excitatory activity in the SON, even when glutamate receptors are blocked (Hatton and Yang, 2002). These actions, as well as direct actions of nicotine, are mediated by α-7 nicotinic receptors on both OT and VP neurons (Zaninetti et al., 2002), and likely underlie the actions attributed to nicotinic activation of VP release (Sladek and Joynt, 1979a; b).

We previously characterized rat PNZ neurons with small somata and very diverse dendritic morphologies using intracellular recording and biocytin labeling in hypothalamo-neurohypophysial explants. Despite this diversity, a commonality in their electrophysiological properties was the relative lack of fast outward rectification coupled with the presence of low threshold depolarizations (Armstrong and Stern, 1997). In the present study we used three strains of transgenic mice to study PNZ neurons containing synthetic enzymes for GABA (glutamate decarboxylase 65 or 67; GAD65 or GAD67), or for acetylcholine (choline acetyltransferase, or ChAT), the promoters of which were tagged with the fluorescent marker enhanced Green Fluorescent Protein (eGFP). We then recorded from identified GAD or ChAT neurons to compare their electrophysiological characteristics with one another, and with unidentified PNZ neurons previously described (Armstrong and Stern, 1997).

Materials and Methods

GAD65-eGFP Expressing Transgenic Mice

Transgenic mice expressing GAD65-eGFP were maintained as a breeding colony by Matthew Ennis at UTHSC, and were originally provided by Gábor Szabó. A description of these mice can be found in López-Bendito et al. (2004), and numerous articles have been published on brain GABAergic anatomy and function using this line (*e.g.,* Bali et al., 2005; Betley et al., 2009; Cui et al., 2011; Parrish-Aungst et al., 2007; Shin et al., 2007; 2011;Wierenga et al., 2010; Zhang et al., 2006). The Szabó lab generated several lines of GAD65 mice- those used here were from line 30, and have been found to substantial overlap in hypothalamus and elsewhere with the known distribution of neurons immunoreactive for GAD or GABA (*e.g.,* Mugnaini and Oertel, 1985).

GAD67-eGFP Expressing Transgenic Mice

Transgenic mice expressing GAD67-eGFP were purchased from Jackson Labs (Bar Harbor, ME; strain CB6-Tg(Gad1-EGFP)G42Zjh/J) and are described in detail on the Jackson Lab web site (http://jaxmice.jax.org/strain/007677.html). They are maintained at UTHSC in a colony by Dr. Fuming Zhou. Like the GAD65 mice, this transgenic line has been used previously (*e.g.*, Ango et al., 2004; Brennaman and Maness, 2008; Starostik et al., 2010).

ChAT-eGFP Expressing Transgenic Mice

Transgenic mice expressing ChAT(BAC)-eGFP were also purchased from Jackson Labs (Bar Harbor, ME; strain: B6.Cg-Tg(RP23-268L19-EGFP)2Mik/J) and were maintained in a colony at UTHSC by Drs. Fuming Zhou and Kazuko Sakata. Details for their development can be found on the Jackson Lab web site (http://jaxmice.jax.org/strain/010802.html). These mice have been

126 used previously to characterize cholinergic neurons (*e.g.,* Ade et al., 2011; Bacskai et al. (2014);
127 Nagy and Aubert, 2012; 2013; Tallini et al., 2006).
128
129 *Slice Preparation*
130 Coronal slices (250 μm) containing the supraoptic nuclei (SON) and surrounding hypothalamus
131 were prepared from mice of either sex (4-6 weeks, 17-20 g). The mice were deeply anesthetized
132 with sodium pentobarbital (50 mg/kg, i.p.) and perfused transcardially with a few ml of ice cold,
133 low-Na^+ (NaCl was replaced by an equiosmolar amount of sucrose) artificial cerebrospinal fluid
134 (ACSF), oxygenated with 95% O_2 and 5% CO_2. The brain was rapidly removed from the skull,
135 immersed in the ice cold ACSF for a few minutes, blocked in the coronal plane and glued to the
136 stage of a vibrating slicer (VT1000s, Leica). The sections were cut into the same sucrose-ACSF
137 slush, transferred to normal ACSF oxygenated continuously at 32-34°C for 1 h, then maintained
138 at room temperature until recording. The ACSF contained (in mM): 125 NaCl, 2.5 KCl, 2 $CaCl_2$,
139 1.0 $MgSO_4$, 1.25 NaH_2PO_4, 26 $NaHCO_3$, 0.45 ascorbic acid, and 20 D-glucose (pH = 7.4; ~290
140 mOsm/kg). Tests with $NiCl_2$ or $CdCl_2$ were performed in phosphate-free ACSF to avoid
141 chelation. The recording chamber was continuously perfused with oxygenated ACSF at
142 ~2ml/min at 32-34°C. Animal procedures were performed under protocols approved by the
143 Institutional Animal Care and Use Committee at University of Tennessee.
144
145 *Electrophysiological Recordings*
146 Whole cell patch-clamp recordings were obtained with an Axon Multiclamp 700A amplifier
147 (Molecular Devices, Inc) and digitized with a Digidata1322, using PClamp 9. Visually directed
148 recordings were made from a modified Olympus BX50WI microscope and a 40x water
149 immersion lens (0.8 n.a.) under IR illumination using a CCD camera (CDD camera (Sensicam,
150 TILL Photonics; now FEI Munich GmbH). GABAergic or cholinergic neurons near the SON

were selected based on their GFP-labeled fluorescence using a Polychrome V monochromator (Till Photonics; now FEI Munich GmbH) with an excitation wavelength of 488 nm. Patch pipettes (4-8 MΩ resistance) were prepared from capillary tubing using a horizontal puller (Sutter Instruments). The pipette solution contained (mM): 140 K-Gluconate, 10 KCl, 10 HEPES, 4 Mg-ATP, 0.3 Na- GTP, 3.5 phosphocreatine and 0.2 EGTA. The pH of the pipette solution was adjusted to 7.4 with 1 M KOH, and osmolarity was adjusted to 285-295 mOsm/kg. The intracellular solutions also contained 0.05-0.1% biocytin (Sigma-Aldrich) to further identify the patched cell. Firing patterns were recorded either at rest or by using small current injections to bring the membrane potential near spike threshold. To measure I/V relations, depolarizing pulses were given from a hyperpolarized (-80 mV) membrane potential; hyperpolarizing pulses were given at a potential just below the threshold of the firing. The duration of the pulses was 400ms. Voltage outputs were filtered at 10 kHz and digitized at 20 kHz. Data were not corrected for a liquid junction potential of ~10 mV.

Immunocytochemistry and Intracellular Labeling in Slices

After recording, the slices were fixed 48-72 hrs at 4°C with 4% paraformaldehyde and 0.2% picric acid in phosphate-buffered saline (PBS). To identify the boundaries of the SON, either an antibody raised in rabbit against VP-neurophysin (VP-NP; 1:20,000; courtesy of Alan Robinson, UCLA), or a monoclonal OT-NP antibody raised in mouse (PS38, 1:500; courtesy of Harold Gainer, NIH) were used. The secondary antibodies used were Alexa Fluor 568-conjugated goat anti-rabbit IgG (for VP staining) or Alexa Fluor 568-conjugated goat anti-mouse IgG (for OT staining) (Invitrogen, Carlsbad, CA).

Because we observed a large number of small and weakly fluorescent ChAT-eGFP neurons, we compared the distribution of ChAT-eGFP neurons with those immunostained with a ChAT

antibody (AB144p; Millipore). The AB144p antibody was raised in goat, used at a dilution of 1:100 and localized with Alexa 568 rabbit anti-goat (Invitrogen), 1:200. This antibody has been extensively characterized and used in over 300 published studies.

To identify the biocytin-filled neurons, slices were then incubated overnight at room temperature with the Avidin-biotin complex (ABC kit, Vector Labs) diluted 1:100 in PBS containing 0.5% Triton-X 100. These slices were reacted with a standard diaminobenzidine staining kit (Vector Labs; Burlingame, CA), rinsed and osmicated for 20 min in 0.05% osmium tetraoxide (in PBS) before mounting on the slides with a polyvinyl alcohol (PVA) solution. This procedure yielded a stable reaction product with minimal tissue shrinkage for photomicrography and drawing. The images from projections through Z stacks shown in Figures 6 and 10 were made with a 20x plan apo objective (0.75 n.a.) on a Nikon Eclipse 90i microscope, using Nikon NIS-Elements software. Filled neurons were reconstructed on a Nikon Optiphot using Neurolucida (Microbrightfield, Inc.) and a 60x water immersion, long working distance objective (Olympus plan apo, 1.2 n. a.).

Confocal Microscopy of GABAergic and Cholinergic eGFP Neurons

Four- to six-week-old GAD65- (n = 3), GAD67- (n = 3) or ChAT- eGFP (n = 4) transgenic mice were anesthetized with sodium pentobarbital (50mg/kg i.p.) and perfused transcardially with 4% paraformaldehyde and 0.2% picric acid in PBS. The brain was removed and immersed in same fixative overnight at 4°C. Coronal or sagittal sections were made with a vibrating slicer (Leica VT 1000s) at 50 μm. Some of the slices were incubated in antibodies to OT-NP, VP-NP or ChAT (as described above). Slices were mounted in PVA. Fluorescent neurons were imaged with a Zeiss 710 confocal microscope. Positive eGFP neurons were viewed with a laser excitation wavelength of 488 nm, whereas neurons immunostained for OT, VP or ChAT, using a

Alexa 568 labeled secondary antibody, were excited with a 561 nm laser line. The images shown in Figures 1, 2, 7 and 8 were taken with a 20x objective (n.a. 0.8). Images of the PVN were tiled to encompass left and right sides in the same micrograph. The qualitative assessment of double-labeling of eGFP neurons with the anti-ChAT was made from individual optical sections through image stacks only as far as the antibody visibly penetrated.

Statistics

Comparisons were made using non-parametric statistics (Wilcoxon Ranked Sum test for two groups, or Kruskal-Wallis non-parametric ANOVA for three groups). Following three-group comparisons, between-group differences were determined with Steel-Dwass Method. Statistics were performed with JMP Pro (SAS Institute Inc.). Differences with a $p \leq 0.05$ were considered significant. Except for some values given for individual neurons as noted, errors listed are s.e.m.

Results

Distribution of GAD65- and GAD67-eGFP Neurons near SON and PVN

In general, the hypothalamic distribution of GAD65 and GAD67 matched well with that described in studies looking at GAD mRNA with *in situ* hybridization (Okamura et al., 1990; Feldblum et al., 1993; Esclapez et al., 1993) and immunoreactivity for GAD or GABA (Mugnaini and Oertel, 1985). Similar to the results of Feldblum et al. (1993), we found many more GAD65 than GAD67 neurons in the mid-anterior regions of the hypothalamus containing the SON and PVN. In particular we found a large number of GAD65-, but very few GAD67-eGFP neurons, in the PNZ of the SON (**Fig. 1**). We found eGFP-expressing cells near and sometimes within the PVN, but again, the majority of these were GAD65 (**Fig. 2**). Although it was previously reported that GAD65 mRNA was found within neurons of the magnocellular component of SON (Feldblum et al., 1993), we typically found GAD65-eGFP only in small

neurons near the SON in the PNZ, but only rarely inside the SON boundaries (*i.e.,* mixed among large OT and VP neurons). Because of the sparse distribution of GAD67-eGFP neurons in the PNZ, we restricted our recordings to labeled neurons in GAD65-eGFP mice.

Electrophysiological Characteristics of GAD65-eGFP Neurons

We characterized some properties of visualized GAD65-eGFP neurons from whole cell, current clamp recordings in coronal slices. Fluorescent neurons were first briefly observed with 488 nm excitation. It was critical that this exposure was brief, as prolonged viewing resulted in either a failure to patch the cell, or in patched cells with the characteristics of damaged neurons (low amplitude, broad spikes, depolarized membrane potential). The effects of prolonged (several min) illumination were also visible with DIC in the most extreme cases, with neurons having a flattened, granular appearance.

Membrane Properties. We recorded from 32 GAD65-eGFP PNZ neurons and an additional 15 eGFP-negative neurons in the same mice. We measured the input resistance (R_n) with a small (+5 mV) voltage step from -70 mV. The average R_n of GAD65-eGFP PNZ neurons was 429.5 $\pm$ 61.5 GΩ, and the range was great (122-1642 GΩ). Small eGFP negative neurons had an R_n of 668.9 $\pm$ 137.4, which was not different from the positive neurons ($p > 0.304$). To compare with PNZ neurons recorded in rats in a previous study (Armstrong and Stern, 1997), we tested neurons with current injection steps at two membrane potentials, one level near spike threshold, another more negative (between -80 and -90 mV). We also passed continuous positive current into neurons that were silent at rest in order to compare their firing pattern with those firing spontaneously. From a hyperpolarized membrane potential, none of the GAD65-eGFP neurons tested exhibited the transient outward rectification in response to depolarizing pulses characteristic of magnocellular SON and PVN neurons (Bourque, 1988; Tasker and Dudek,

1991; Armstrong and Stern, 1997), and all but two of 35 tested showed a depolarizing hump that emerged beneath the fast spike threshold, consistent with the presence of a low-threshold spike (LTS) similar to that observed in some PVN parvocellular neurons (Tasker and Dudek, 1991) and PNZ neurons in the rat (Armstrong and Stern, 1997) (**Fig. 3A**). In 8/11 eGFP-negative neurons, the LTS was also evoked by this test. As shown in Fig. 3A, the LTS could sometimes reach fast spike threshold, generating multiple fast, large amplitude spikes.

When neurons were hyperpolarized in current steps from a depolarized membrane potential below spike threshold (between -50 and -60 mV), 19/23 GAD65-eGFP neurons tested showed a depolarizing sag indicating an inward rectification (**Fig. 3B**) with 6/7 eGFP-negative neurons tested showing a similar response-characteristic of an I_h-type current. The I/V response for neurons without inward rectification was relatively linear. At the offset of the most negative hyperpolarizing pulses, a rebound LTS was also present in all neurons (**Fig. 3B**). In 5/5 neurons tested, the LTS and rebound remained after blocking fast Na^+ spikes with 0.5 μM TTX (**Fig. 4**).

In many cases, an LTS similar to what we observed in PNZ neurons is mediated by low threshold Ca^{++} currents (see Perez-Reyes, 2003, for review). To determine the Ca^{++}-dependence of the LTS in PNZ neurons, we first tested 100 μM $NiCl_2$ (n = 13), since 50-100 μM $NiCl_2$ has been shown to block low threshold Ca^{++} currents in the SON (Fisher and Bourque, 1995; Israel et al., 2008), and in parvocellular PVN neurons (Luther and Tasker, 2000). However, 100 μM $NiCl_2$ failed to block or even strongly reduce the LTS in any of these 13 neurons, including 3 neurons tested after TTX (**Fig. 4A-C**). The effectiveness of $NiCl_2$ at blocking some currents could be observed however, by its ability to reduce spontaneous synaptic activity (**Fig. 4D, E**). Unfortunately, when we exposed neurons to $CdCl_2$ (200 μM; n = 7) to further study the Ca^{++}

dependence of the LTS, the recordings consistently became unstable and we could not complete this assessment.

Firing Properties. Firing rate and spike distribution were examined from 1-2 min records. Over one-half (21/35) of GAD65-eGFP neurons were spontaneously active with a mean firing rate of 6.3 $\pm$ 0.74 Hz and a coefficient of variation (CV) for interspike intervals (ISI) of 1.07 $\pm$ 0.22. These neurons could be loosely grouped into 7 neurons that fired in an irregular pattern (CV 0.32-0.77; firing rate 3.3-9.7 Hz), 8 bursting neurons, firing bursts of action potentials on an irregular background pattern or phasically with little firing in between (CVs > 1), and 6 neurons that fired in a more regular, continuous pattern (CV 0.06-0.15; firing rate 5.5-12.9 Hz) (**Fig. 5**). Following continuous depolarizing current injection in another 11 neurons tested, 8 fired irregularly, and 3 fired with bursts. The remaining silent neurons were not tested for firing pattern but all exhibited action potentials upon depolarization. We also recorded from 11 small PNZ neurons that did not express eGFP. Of these 9 fired spontaneously, with a mean firing rate of 7.2 $\pm$ 1.79 Hz and an ISI CV of 1.19 $\pm$ 0.42 (not shown). Most of these 9 fired in an irregular pattern (n = 6; CV 0.32-0.62; firing rate 4-9.1 Hz), and a few irregularly with bursts (n = 3; CV 1.23-3.33; firing rate 4.4-18.7 Hz), patterns similar to those shown in **Fig. 5B** and **C**. None showed a highly regular pattern. Overall, there were no differences between spontaneously firing eGFP positive and eGFP negative neurons with regards to firing rate ($p > 0.7687$) or CV ($p > 0.9223$).

Morphological characteristics of filled GAD65-eGFP neurons

We filled 17 GAD65-eGFP neurons with biocytin. Two examples are shown **in Fig. 6**. These neurons were similar to those filled earlier with sharp electrodes in hypothalamic explants (Armstrong and Stern, 1997), with fusiform or rounded somata. Most of the neurons had long,

thin processes that, in the coronal plane, extended long distances over the SON laterally and medially. While occasionally these processes would pass through the nucleus, we found no apparent terminal processes in the SON. Distinguishing dendrites from axons was often difficult due to the thinness of these processes and also to the paucity of visible spines, and many of the identified axons appeared cut near the soma. Thus not only did we not view any processes terminating in the SON, terminal arborizations were not apparent, suggesting these neurons have projections well beyond the coronal slice. Filled GAD65 neurons exhibited 3.7 $\pm$ 0.39 primary dendrites, 7.8 $\pm$ 0.9 branches, a dendritic length of 1606 $\pm$ 189 μm, and a somatic area of 185.1 $\pm$ 18.6 μm.

Distribution of ChAT Neurons

We found two populations of ChAT-eGFP neurons in hypothalamus near the SON. One population had large somata (>20 μm) with multiple dendrites, were brightly eGFP-positive, and appeared to be part of the canonical group of basal forebrain/diencephalic cholinergic neurons as visualized with choline acetyltransferase immunohistochemistry (Armstrong et al., 1983; Houser et al, 1983; Woolf et al., 1983). In the PNZ, most of these large neurons lay dorsolateral to the SON, contained in the ventrolateral portion of the lateral and magnocellular preoptic areas and horizontal limb of the diagonal band of Broca (HLDB) rostrally, and caudally in the lateral hypothalamus and substantia inominata. Some of these large eGFP neurons were found immediately adjacent to magnocellular neurons stained for VP- or OT-NP (**Fig. 7).** As described originally by Mason and co-workers (Mason et al, 1983; Theodosis and Mason, 1988), some of these large ChAT neurons had processes that projected into the SON (**Fig. 7B**). Large ChAT-eGFP neurons were not observed near the PVN.

A second population of smaller ChAT-eGFP neurons, with a much dimmer fluorescence, was distributed extensively in the rostral hypothalamus, including the PNZ (**Fig. 7**). These weaker ChAT-eGFP neurons were also observed in the medial part of the PVN, the posterior hypothalamic nucleus immediately caudal to the PVN, and in various parts of the mammillary complex. The processes of many of the small ChAT-eGFP neurons were difficult to visualize due to the weaker fluorescence. A very small minority of the smaller ChAT-eGFP-positive somata appeared as bright as the larger neurons. In general, fewer of these smaller neurons were located in the posterior parts of the hypothalamus- the ventromedial nucleus was noticeably devoid of eGFP somata. Other neurons well known to be cholinergic besides those in the basal forebrain, like those of the medial habenula and their axons in fasciculus retroflexus projecting to the interpeduncular nucleus, were strongly eGFP-positive.

We incubated hypothalamic slices from two ChAT-eGFP mice with the affinity purified AB144p polyclonal antibody to determine if both the brightly and more weakly fluorescent populations of ChAT-eGFP neurons would react for ChAT. Immunofluorescence with this antibody was robust and the pattern of stained neurons fit that of the canonical ChAT distribution of the basal forebrain mentioned above (as well as the medial habenula), and included many double-labeled neurons. Only eGFP neurons within the same focal plane of anti-ChAT neurons were considered for double labeling, since antibody penetration may not be complete in the middle of the section. Double-labeled neurons in the PNZ lay rostrally in the medial parts of the lateral and magnocellular preoptic areas, and the HLDB. Caudally the PNZ included the ventromedial aspects of the lateral hypothalamus and the substantia inominata, both of which also had a large number of large, bright ChAT-eGFP neurons that were double-labeled for ChAT immunoreactivity. In contrast, the smaller, weakly fluorescent eGFP neurons in the PNZ were

not double labeled. (**Fig. 8**). A few of the small neurons were as bright as the large eGFP neurons, but these also did not stain for anti-ChAT.

There were hypothalamic and adjacent regions with smaller eGFP neurons that did double label for anti-ChAT. Posteriorly, there was double labeling in the posterior hypothalamic nucleus, and some parts of the mammillary complex, especially the supramammillary nucleus. A small number of neurons appeared to react for anti-ChAT but did not express eGFP, such as some in the lateral part of the arcuate nucleus. In the adjacent amygdala, a dense, apparently axonal innervation of the basolateral amygdala was visible with both anti-ChAT and ChAT-eGFP double-labeled processes. We found some scattered ChAT-eGFP somata in this region as well, but these neurons did not react with anti-ChAT. In conclusion, the great majority of the small ChAT-eGFP neurons in hypothalamus, including those in the PNZ, were not labeled for anti-ChAT.

Electrophysiological Characteristics of ChAT-eGFP Neurons

Membrane Properties. We recorded 9 large and brightly fluorescent cells, and 12 of the smaller, weakly fluorescent ChAT-eGFP neurons. The larger ChAT-eGFP neurons had an input resistance of 216.4 $\pm$ 47.2 MΩ, significantly smaller than that of the smaller neurons (1406.0 $\pm$ 231.4 MΩ; $p \leq 0.0002$). The majority (8/9) of the larger neurons did not fire spontaneously, having an average resting potential (-56.3 $\pm$ 1.9 mV) which was below spike threshold. In contrast, the majority of the smaller neurons fired spontaneously (see below). All 9 of the large ChAT-eGFP neurons were characterized by a transient outward rectification, revealed either with depolarizing pulses when holding the neuron negative, as in **Fig. 9A**, or at the offset of hyperpolarizing pulses when given from a more depolarized membrane potential, as in **9C**. Seven of these neurons also exhibited a delayed, transient depolarization like that shown in **9A**,

but this was much smaller than the LTS observed in parvocellular neurons. In contrast, similar to parvocellular neurons in the GAD65-eGFP mice, 9 of the 11 weakly fluorescent, smaller ChAT-eGFP neurons tested were characterized by a prominent LTS either when depolarized from a hyperpolarized holding potential, as in **Fig. 9B**, or at the offset of hyperpolarizing pulses from a more depolarized membrane potential, as **in Fig. 9D**, and showed very little transient outward rectification. About half of the cells of each type exhibited some inward rectification when hyperpolarized to quite negative membrane potentials ($\leq$ -80 mV). Another marked difference between the larger ChAT-eGFP neurons and the smaller cells was in the size of the spike hyperpolarizing afterpotential (HAP) which was significantly bigger in the larger neurons (-20.8 $\pm$ 1.3 mV) compared to the smaller cells (-7.7 $\pm$ 0.8 mV; $p \leq 0.0001$) (**Fig. 9).**

Firing Properties. Eleven of the 12 smaller, weakly fluorescent neurons fired spontaneously, and most (n = 10) exhibited patterns similar to those of the irregular firing parvocellular neurons in the GAD65-eGFP mouse (firing rate = 6.4 $\pm$ 0.7 Hz; CV = 0.45 $\pm$ 0.06) shown in **Fig. 5.** One neuron fired regularly (CV = 0.20; firing rate 9.3 Hz). Bursting neurons were not observed.

Although 8/9 of the larger ChAT-eGFP neurons were silent at rest, they could be depolarized to elicit spike trains. When depolarized to threshold, these 9 neurons fired slowly with a mean rate of 2.8 $\pm$ 0.2 Hz and a CV of 0.89 $\pm$ 0.14. Most (n = 5) of these neurons fired very irregularly (CV 0.55-0.95), but three exhibited bursting patterns (CV 1.06-1.69), and one fired in a highly regular fashion (CV = 0.11). Thus this variability suggests that, like the smaller neurons recorded from the GAD65 mice, firing pattern alone would not distinguish cell types. And although only one large ChAT-eGFP neuron fired spontaneously, this was also true of about 60% of the GAD65-eGFP neurons, so electrical silence is also not a reliable signature.

Morphological Characteristics of Filled ChAT-eGFP Neurons

Large ChAT-eGFP Neurons. The 9 large ChAT-eGFP neurons we filled with biocytin and reconstructed were characterized by somata that were 324.0 ± 29.2 μm in area, 4.4 ± 0.4 primary dendrites with 12.7 ± 1.5 branches, and a total dendritic length of 1363.0 ± 249.8 μm. Examples are shown in **Fig. 10A, B, D, and E**. These neurons had large (>20 μm) polygonal or rounded somata. Most of the dendrites were smooth, often varicose, and not particularly spiny. One or two of the primary dendrites were typically thicker than the other dendrites proximally. Spines were more often found on the distal parts of the dendrite, but in general, these neurons would not be characterized as spiny. These neurons were on average located more dorsolateral to the SON, but could be found along its rostro-caudal length. In contrast to GAD65-eGFP neurons which had medio-laterally oriented dendrites, large ChAT-eGFP neurons had their dendrites dorso-ventrally oriented. The majority of these neurons had extensive axonal arbors that ramified locally (**Fig. 10D, E**). However, while dendrites and axons occasionally encroached on the border of the SON, no obvious innervation was noted.

Small ChAT-eGFP Neurons. In contrast, the 8 filled smaller ChAT-eGFP neurons (soma area = 117.6 ± 13.7 μm) exhibited only 2.5 ± 0.5 primary dendrites, with 4.0 ± 1.2 branches, and a total length of 531.7 ± 215.2 μm. The somata of these neurons were rounded or fusiform in shape. Three examples are shown in **Fig**. **10C**. Although soma size was similar to GAD65-eGFP neurons, the dendritic trees of these neurons were much less extensive, having fewer primary dendrites, fewer branches and only about one-third of the total dendritic length, suggestive of a different morphological phenotype. The dendrites of the smaller neurons were seldom spiny, and often varicose. Thus, although similar in some electrophysiological properties to GAD65-eGFP neurons (like the LTS), these two neuron types had morphologies very different from another.

Morphological Comparisons Across Cell Types

A comparison of the two ChAT-eGFP groups with the filled GAD65-eGFP neurons revealed several differences. Not surprisingly, the three groups differed in soma area ($p \leq 0.0002$), with both parvocellular neurons significantly smaller than large ChAT-eGFP neurons ($p = 0.0018$ for small ChAT neurons; $p = 0.0035$ for GAD65-eGFP neurons). There was a difference in the number of primary dendrites ($p \leq 0.0104$) that was only significant between the small and large ChAT-eGFP neurons ($p = 0.025$). The number of branches differed ($p \leq 0.0014$), with between group comparisons showing that large ChAT-eGFP neurons had the most branches compared to either the small ChAT-eGFP neurons ($p = 0.0078$) or the GAD65-eGFP neurons ($p = 0.0396$). Interestingly, GAD65-eGFP neurons had more branches than small ChAT-eGFP neurons ($p = 0.0467$). Total dendritic length also varied significantly across groups ($p < 0.0072$). However, unlike branching, there was no difference in dendritic length between GAD65-eGFP and the large ChAT-eGFP neurons, whereas small ChAT-eGFP neurons had much smaller dendritic trees than either GAD65-eGFP ($p = 0.013$) or large ChAT-eGFP ($p = 0.0483$).

Discussion

With the advantage of transgenic mice labeled for the synthetic enzymes for GABA and acetylcholine, we have been able to extend our original observations of unidentified PNZ neurons by comparing the morphology and electrophysiology of these two classes of neurons near the rodent SON. Our findings suggest these broad results: 1) the three groups of parvocellular neurons we examined in this region overwhelmingly possess an LTS, but otherwise differ in morphology; 2) secondly and not surprisingly, large ChAT neurons exhibit very different characteristics from the smaller PNZ neurons; and 3) as in our previous investigation using sharp electrode recordings from unidentified neurons in the rat PNZ (Armstrong and Stern,

1997), we were unable to demonstrate direct axonal terminal-type innervation from this region to the SON; however, reconstructions were done from slices and processes were undoubtedly severed. In contrast, as will be discussed below, processes, probably both axons and dendrites, did encroach on the SON.

Expression of GAD65-eGFP and GAD67-eGFP in the PNZ

The expression of GAD65-eGFP neurons, which we found much more plentiful than GAD67 in hypothalamus and adjacent structures, reasonably matched previous studies using *in situ* hybridization in rat (also see Feldlblum et al., 1993). This included a large number of neurons in the anterior nucleus and medial hypothalamus, medial preoptic area, suprachiasmatic nucleus, zona incerta, and bed nucleus of the stria terminalis, the latter of which also contained numerous GAD67 neurons (Okamura et al., 1990; Cullinan et al., 1993; Feldblum et al., 1993; Roland and Sawchenko, 1993). Within the PNZ, scattered GAD-positive or GABA-positive neurons also have been observed immunochemically (Herbison, 1994; Iijima et al., 1986; Theodosis et al., 1986). While not densely distributed, the GAD65 neurons nevertheless were plentiful and easily located in the PNZ in all slices, where they lay more dorsolateral than dorsomedial, at the ventral aspect of the lateral hypothalamus. Some neurons encroached on the dorsal aspect of the SON, but these were very sparse and typically not as brightly fluorescent as those clearly more dorsal in the PNZ. Some of these may correspond to putative GABA neurons containing GABA transaminase described by Iijima and Kojima (1985) in the SON. Similarly, we noted only a few small GAD65-eGFP neurons within the PVN proper, but these neurons were very densely distributed proximal to the PVN, especially dorsally in the zona incerta, and ventrolaterally in the subparaventricular zone.

Electrical Properties of GAD65-eGFP Neurons

The line of transgenic mice we used has been valuable in characterizing developmental, morphological and electrophysiological attributes of GABAergic neurons in many areas of brain and spinal cord since its creation in 2004 (López-Bendito et al., 2004), and single cell polymerase chain reaction has verified GAD67 and/or GAD65 mRNA in many eGFP-positive neurons in the anterior hypothalamus and zona incerta (Shin et al., 2007); some of these GABAergic neurons expressed an LTS. GABAergic neurons in the lateral hypothalamus (LH) also have been extensively characterized both morphologically and electrophysiologically in these mice (Karnani et al., 2013). Lateral hypothalamic GAD65 neurons are electrophysiologically diverse, with at least 4 types identified, only one of which has an LTS with a profile similar to the great majority of PNZ GABAergic neurons. Karnani et al. (2013) found that LTS neurons in the LH accounted for one quarter of the GABAergic neurons sampled, but were similar morphologically to the regular spiking, fast spiking, and late spiking LH cell types. Thus while PNZ GABAergic neurons are characterized by an LTS, this is not the case for other hypothalamic GABAergic neurons, and certainly not the case for a great many GABAergic neuron types in the central nervous system. In the anterior hypothalamic nucleus, most GABAergic neurons from normal mice did not exhibit an LTS, but a majority did after adrenalectomy and a steroid treatment selectively activating mineralcorticoid receptors (Shin et al., 2011). It is not known whether mineralcorticoid receptors are also found in GABAergic PNZ neurons *per se*, but they are found in this region as well as in SON magnocellular neurons, and in many other parvocellular neurons in the hypothalamus, especially those near the PVN (Teruyama et al., 2012).

In some regions of the brain, LTS profiles similar to those we observed are blocked or strongly suppressed by low (50-100 μM) concentrations of Ni^{++}, compatible with the expression of at least one class of T-type Ca^{++} channels (CaV 3.2) (Perez-Reyes, 2003). In hypothalamus, this

498 appears the case for the LTS and the T-current found in one class of parvocellular PVN neurons
499 (Luther and Tasker, 2000) and in magnocellular neurons in the SON (Fisher and Bourque, 1995;
500 Israel et al., 2008). However in other cases, the LTS or T-current may be sensitive only to higher
501 concentrations of Ni^{++} (Perez-Reyes, 2003). In hypothalamus, such neurons include those in the
502 guinea pig SON (Erickson et al., 1993), magnocellular dorsal nucleus (Niespodziany et al., 1999)
503 and in rat ventromedial nucleus (Akaike et al., 1989). However, the underlying Ca^{++} channels in
504 all these cases have not been determined. While the LTS in the PNZ GAD65-eGFP neurons
505 remained following TTX, it was not blocked by 100 μM $NiCl_2$, suggesting an underlying
506 channel type different from CaV3.2. It is unclear why the neurons we tested with $CdCl_2$ became
507 unstable, despite precautions to avoid chelation. In similar experiments recording from SON
508 magnocellular neurons, this problem was not encountered with 200 μM $CdCl_2$ (Teruyama and
509 Armstrong, 2005), and even with concentrations as high 500 μM (Stern and Armstrong, 1997).
510 As for the characteristics of the LTS itself, there seemed little difference between the GAD65-
511 eGFP positive and negative neurons, or from what we observed previously in unidentified
512 neurons (Armstrong and Stern, 1997). With regard to firing pattern, a range was observed, with
513 an emphasis on irregularly firing and some bursting neurons. However, a regular, oscillatory
514 bursting pattern characteristic of some neurons with an LTS, such those in thalamus (*e.g.,*
515 Huguenard and Prince, 1992; Kim and McCormick, 1998), was not observed. However this
516 pattern is likely highly voltage-dependent and possibly network driven, thus its absence in our
517 recordings must be viewed with caution.
518
519 *Morphology of GAD65-eGFP Neurons*
520 While the morphology of many GAD65-eGFP neurons resembled some of the unidentified PNZ
521 neurons we previously reconstructed from hypothalamic explants (Armstrong and Stern, 1997),
522 the use of slices restricted visualization of extended processes compared to the explant. Notable

however was that most of the neurons we filled in the current study were aspiny, compared to the ~50% of neurons filled intracellularly in the explant that were densely spiny. While many of the neurons had extensive processes projecting medio-laterally, similar to a majority of the neurons in the first study, the same degree of axonal or dendritic branching was not apparent, most likely due to the restricted dimension of the slice vs. explants, although we cannot rule out a difference between rats and mice. In general, the neurons in the present study had a more homogenous morphology, most similar to the aspiny neurons from the first study. In neither study could we verify a local, terminal projection to the SON, even though processes passed near or even with SON boundaries in both cases. Since processes in passage, either dendritic or axonal, may take up extracellular tracers, it remains unsettled whether PNZ neurons are a major source of the extensive GABAergic innervation of the SON.

Expression of ChAT-eGFP in the PNZ

The brightest, larger ChAT-eGFP neurons near the SON appeared part of the canonical, basal forebrain cholinergic system, the most ventral and caudal aspects of which included the PNZ in the lateral hypothalamus (Armstrong et al., 1983; Houser et al, 1983; Woolf et al., 1983). These neurons were overwhelmingly positive for anti-ChAT. In contrast, the numerous smaller ChAT-eGFP neurons in the PNZ, the great majority of which were dimly fluorescent, were not immuonoreactive. In general, the number of smaller hypothalamic eGFP neurons we observed seemed much greater than previously reported for anti-ChAT reactive cells. However, some immunochemical studies have reported a relatively broad distribution of ChAT-positive neurons in rat hypothalamus, including many smaller neurons (Rodriquez-Sierra and Morley; 1985; Rao et al., 1987; Tago et al., 1987). Similar to Rao et al. (1987), we observed ChAT-eGFP neurons immunolabeled for ChAT in the posterior hypothalamic nucleus and in parts of the mammillary complex. We did not observe ChAT-eGFP neurons in the arcuate nucleus, although a few

548 neurons in the lateral aspects of the arcuate were immunolabeled for ChAT alone. Probably
549 owing to the use of different antibodies, arcuate neurons have been reported as both cholinergic
550 (Rao et al., 1987; Tago et al. (1987) and non-cholinergic (Rodriquez-Sierra and Morley, 1985).
551 Thus we cannot corroborate whether the small PNZ ChAT-eGFP neurons we observed were
552 truly cholinergic, nor can we exclude this possibility. What is clear however, is the marked
553 difference in the electrophysiological properties of the large neurons that were double labeled,
554 and these smaller neurons that were only eGFP positive.
555
556 *Electrical Properties of ChAT-eGFP Neurons*
557 The larger ChAT-eGFP neurons we recorded differed from the parvocellular PNZ types,
558 including GAD65-eGFP neurons, by exhibiting: 1) a prominent transient outward rectification
559 that delayed spiking when neurons were depolarized from a relatively hyperpolarized membrane
560 potential; 2) a large spike hyperpolarizing afterpotential; and 3) having a weak transient
561 depolarizing potential, smaller than the LTS recorded in parvocellular neurons. In general, our
562 results are in good agreement with those of Hedrick and Waters (2010) who recorded from
563 immunochemically identified ChAT neurons in mice; others have also reported strong transient
564 outward rectification in ChAT neurons in septum and nucleus basalis (Markram and Segal, 1990;
565 Khateb et al., 1992). However, in some studies forebrain ChAT neurons, especially those in
566 guinea pig, have also been found to exhibit a prominent LTS and/or a high density of T-channels
567 (Alonso et al., 1996; Han et al., 2005; Gorelova and Reiner, 1996; Khateb et al. 1992). While the
568 great majority of the more dimly fluorescent, smaller ChAT-eGFP neurons exhibited little
569 transient outward rectification and a prominent LTS- very similar to the GAD65-eGFP positive
570 and negative parvocellular neurons. The transient, delayed depolarization we observed in large
571 ChAT-eGFP positive neurons did not produce bursts of spikes. The expression of an LTS would
572 likely be competitive with the strong transient outward rectification, so its possible that large

mouse ChAT neurons have the underlying T-type or related inward currents superimposed on an I_a type current. The small ChAT-eGFP neurons exhibited electrical properties largely indistinguishable from GAD65-eGFP neurons, or the eGFP-negative neurons we studied in those animals.

Morphology of ChAT-eGFP Neurons

Our results from filling the larger ChAT-eGFP neurons closely resemble those from the Golgi study of Dinopoulos et al. (1988), who described about 50% of basal forebrain neurons as having large polygonal or triangular somata with three to five dendrites possessing several branches- this description also matches that of identified cholinergic neurons in the same general region of guinea pig basal forebrain by Alonso et al. (1996) and Manns et al. (2000). Like previous studies, we found the dendrites of most neurons to be relatively smooth, often varicose, and only occasionally studded with spines. With the exception of possessing more spines, similar ChAT-positive neurons were described in ventral pallidum by Bengston and Osborne (2000). Dinopoulos et al. (1988) also found neurons in nucleus basalis with smaller rounded or fusiform somata that had much less extensive dendritic trees, reminiscent of the smaller neurons we observed for the smaller ChAT-eGFP neurons. However, the non-cholinergic neurons studied by Alonso et al. (1996) in substantia inominata were not very different in size or in dendritic morphology from their ChAT-positive neurons, but were found generally ventral to the latter. The smaller ChAT neurons from which we recorded had morphologies different from both the GAD-65 neurons and the larger ChAT neurons, with a much more restricted dendritic tree, both in the numbers of primary dendrites, as well as the extension of these dendrites, than either of these other cell types. Thus these smaller ChAT-eGFP neurons did not appear to represent an overlap with the GABAergic population.

598 *Firing Properties of PNZ Neurons*

599 In general, the spontaneous firing patterns of the parvocellular neurons we recorded would not be
600 useful for distinguishing the various cell types. A great diversity was found in the GAD65-eGFP
601 neurons, 40% of these being silent, and of the spontaneously firing neurons, patterns ranged from
602 regular to irregular and of the latter, included many bursting neurons. Although regular bursting
603 activity has previously been associated with an LTS in cholinergic neurons in guinea pig (Khateb
604 et al., 1992) and broadly in thalamic neurons (see Contreras, 2006 for review), we found no such
605 activity. However, repetitive bursting in other LTS neurons is often the result of network activity
606 (Kim and McCormick 1998), and even when not, is voltage-dependent: LTS neurons in striatum
607 for example, can exhibit a range of autonomous firing patterns, from regular non-bursting to
608 irregular firing, irregular bursts, and regular bursting, all depending on membrane potential
609 (Beatty et al., 2012).

610

611 The largest difference we noted among the various cell types was that only 1 of 9 large ChAT
612 neurons fired spontaneously, compared to GAD65-eGFP neurons, small eGFP-negative neurons,
613 and small ChAT-eGFP neurons, where spontaneous activity was present in 60-90% of the cells.
614 Even when prompted to fire, the larger ChAT-eGFP neurons fired more slowly that the smaller
615 PNZ cell types, but could exhibit patterns of activity (regular, irregular, bursting) that would be
616 indistinguishable from the smaller cell types, including those recorded in the GAD65-eGFP
617 mice. The low amount of spontaneous activity we observed in the larger ChAT neurons is
618 consistent with a previous study in mouse (Hedrick and Waters, 2010).

619

620 *A Cautionary Note for Dissociated SON Preparations Regarding Cholinergic Neurons*

621 Magnocellular SON neurons (Bourque, 1988), especially VP cells (Stern and Armstrong, 1996;
622 Fisher et al., 1998), exhibit a strong transient outward rectification that distinguishes them from

nearby parvocellular neurons. A similar distinction has been noted between the magnocellular neurosecretory and other neurons in the PVN, where neurosecretory parvocellular neurons, while exhibiting little transient outward rectification, do not exhibit the LTS characteristic of pre-autonomic PVN neurons (Luther et al., 2002; Stern, 2001). As elsewhere in the brain, dissociated cell preparations of the SON have proved valuable for the initial characterizations of a variety of ion channel currents due to favorable space clamp. In general, these neurons were chosen on the basis of their large size, which correlated with larger size of identified magnocellular OT or VP neurons; these large neurons were characterized by prominent transient outward rectification (Oliet and Bourque, 1992). Fisher and Bourque (1998) later characterized the underlying A-type potassium current in identified OT and VP neurons. However, the close proximity of some of the ChAT neurons to the SON, their similarly large somata, and their prominent transient outward rectification, means that without immunochemical or some supplementary verification of their neurosecretory phenotype, they could be mistaken for OT or VP neurons. Although on average SON neurons have fewer (2-3) primary dendrites than do the ChAT neurons (4-5 dendrites), there are some magnocellular neurons with as many as 4-5 primary dendrites (Randle et al., 1986; Smith and Armstrong, 1990; Armstrong, 1995; Stern and Armstrong, 1998) and three of the 9 ChAT neurons we filled had only 3 primary dendrites. Finally, the dissociation procedure typically insures that the original dendritic morphology will not be represented in the acutely isolated neuron.

Acknowledgements

This work was supported by NIH grants R56NS23941 and R01HD072056 (WEA). We thank Fuming Zhou and Kazuko Sakata for maintaining the transgenic GAD67 and ChAT-eGFP mice used in this study, and Dr. Robert Foehring for commenting on a previous version of the manuscript.

References

Ade KK, Wan Y, Chen M, Gloss B, and Calakos N. An Improved BAC Transgenic Fluorescent Reporter Line for Sensitive and Specific Identification of Striatonigral Medium Spiny Neurons. *Front Syst Neurosci* 5: 32, 2011.

Akaike N, and Kaneda M. Glycine-gated chloride current in acutely isolated rat hypothalamic neurons. *J Neurophysiol* 62: 1400-1409, 1989.

Alonso A, Khateb A, Fort P, Jones BE, and Muhlethaler M. Differential oscillatory properties of cholinergic and noncholinergic nucleus basalis neurons in guinea pig brain slice. *Eur J Neurosci* 8: 169-182, 1996.

Ango F, di Cristo G, Higashiyama H, Bennett V, Wu P, and Huang ZJ. Ankyrin-based subcellular gradient of neurofascin, an immunoglobulin family protein, directs GABAergic innervation at Purkinje axon initial segment. *Cell* 119: 257-272, 2004.

Armstrong DM, Saper CB, Levey AI, Wainer BH, and Terry RD. Distribution of cholinergic neurons in rat brain: demonstrated by the immunocytochemical localization of choline acetyltransferase. *J comp Neurol* 216: 53-68, 1983.

Armstrong WE. Morphological and electrophysiological classification of hypothalamic supraoptic neurons. *Prog Neurobiol* 47: 291-339, 1995.

Armstrong WE. Hypothalamic Supraoptic and Paraventricular Nuclei. In: *The Rat Nervous System*, 4th Edition, edited by Paxinos G. Sydney: Elsevier, 2014, in press.

Armstrong WE, and Stern JE. Electrophysiological and morphological characteristics of neurons in perinuclear zone of supraoptic nucleus. *J Neurophysiol* 78: 2427-2437, 1997.

Bacskai T, Rusznak Z, Paxinos G, and Watson C. Musculotopic organization of the motor neurons supplying the mouse hindlimb muscles: a quantitative study using Fluoro-Gold retrograde tracing. *Brain Struct Funct* 219: 303-321, 2014.

Bourque CW. Transient calcium-dependent potassium current in magnocellular neurosecretory cells of the rat supraoptic nucleus. *J Physiol (Lond)* 397: 331-347, 1988.

Bali B, Erdelyi F, Szábo G, and Kovacs KJ. Visualization of stress-responsive inhibitory circuits in the GAD65-eGFP transgenic mice. *Neurosci Lett* 380: 60-65, 2005.

Beatty JA, Sullivan MA, Morikawa H, and Wilson CJ. Complex autonomous firing patterns of striatal low-threshold spike interneurons. *J Neurophysiol* 108: 771-781, 2012.

Betley JN, Wright CV, Kawaguchi Y, Erdelyi F, Szábo G, Jessell TM, and Kaltschmidt JA. Stringent specificity in the construction of a GABAergic presynaptic inhibitory circuit. *Cell* 139: 161-174, 2009.

Bengtson CP, and Osborne PB. Electrophysiological properties of cholinergic and noncholinergic neurons in the ventral pallidal region of the nucleus basalis in rat brain slices. *J Neurophysiol* 83: 2649-2660, 2000.

Boudaba C, Schrader LA, and Tasker JG. Physiological evidence for local excitatory synaptic circuits in the rat hypothalamus. *J Neurophysiol* 77: 3396-3400, 1997.

Brennaman LH, and Maness PF. Developmental regulation of GABAergic interneuron branching and synaptic development in the prefrontal cortex by soluble neural cell adhesion molecule. *Mol Cellular Neurosci* 37: 781-793, 2008.

Bruni JE, and Perumal PM. Cytoarchitecture of the rat's supraoptic nucleus. *Anat Embryol* 170: 129-138, 1984.

Contreras D. The role of T-channels in the generation of thalamocortical rhythms. *CNS & Neurol Disord Drug Targets* 5: 571-585, 2006.

Cullinan WE, Herman JP, and Watson SJ. Ventral subicular interaction with the hypothalamic paraventricular nucleus: evidence for a relay in the bed nucleus of the stria terminalis. *J comp Neurol* 332: 1-20, 1993.

Cui L, Kim YR, Kim HY, Lee SC, Shin HS, Szábo G, Erdelyi F, Kim J, and Kim SJ. Modulation of synaptic transmission from primary afferents to spinal substantia gelatinosa neurons by group III mGluRs in GAD65-EGFP transgenic mice. *J Neurophysiol* 105: 1102-1111, 2011.

Dinopoulos A, Parnavelas JG, Uylings HB, and Van Eden CG. Morphology of neurons in the basal forebrain nuclei of the rat: a Golgi study. *J comp Neurol* 272: 461-474, 1988.

Dyball REJ, and Kemplay SK. Dendritic trees of neurones in the rat supraoptic nucleus. *Neuroscience* 7: 223-230, 1982.

Erickson KR, Ronnekleiv OK, and Kelly MJ. Role of a T-type calcium current in supporting a depolarizing potential, damped oscillations, and phasic firing in vasopressinergic guinea pig supraoptic neurons. *Neuroendocrinology* 57: 789-800, 1993.

Esclapez M, Tillakaratne NJK, Tobin AJ, and Houser CR. Comparative localization of mRNAs encoding two forms of glutamic acid decarboxylase with nonradioactive in situ hybridization methods. *J comp Neurol* 331: 339-362, 1993.

Feldblum S, Erlander MG, and Tobin AJ. Different distributions of GAD-65 and GAD-67 mRNAs suggest that the two glutamate decarboxylases play distinctive functional foles. *J Neurosci Res* 34: 689-706, 1993.

Felten DL, and Cashner KA. Cytoarchitecture of the supraoptic nucleus. *Neuroendocrinology* 29: 221-230, 1979.

Fisher TE, and Bourque CW. Voltage-gated calcium currents in the magnocellular neurosecretory cells of the rat supraoptic nucleus. *J Physiol (Lond)* 486: 571-580, 1995.

751 **Fisher TE, Voisin DL, and Bourque CW**. Density of transient K+ current influences
752 excitability in acutely isolated vasopressin and oxytocin neurones of rat hypothalamus. *J Physiol*
753 *(Lond)* 511: 423-432, 1998.
754
755 **Gorelova N, and Reiner PB**. Role of the afterhyperpolarization in control of discharge
756 properties of septal cholinergic neurons in vitro. *J Neurophysiol* 75: 695-706, 1996.
757
758 **Han SH, Murchison D, and Griffith WH**. Low voltage-activated calcium and fast
759 tetrodotoxin-resistant sodium currents define subtypes of cholinergic and noncholinergic neurons
760 in rat basal forebrain. *Brain Res: Mol Brain Res* 134: 226-238, 2005.
761
762 **Hatton GI, and Yang QZ**. Synaptic potentials mediated by alpha 7 nicotinic acetylcholine
763 receptors in supraoptic nucleus. *J Neurosci* 22: 29-37, 2002.
764
765 **Herbison AE**. Immunocytochemical evidence for oestrogen receptors within GABA neurones
766 located in the perinuclear zone of the supraoptic nucleus and GABAA receptor beta 2/beta 3
767 subunits on supraoptic oxytocin neurones. *J Neuroendocr* 6: 5-11, 1994.
768
769 **Hedrick T, and Waters J**. Physiological properties of cholinergic and non-cholinergic
770 magnocellular neurons in acute slices from adult mouse nucleus basalis. *PloS one* 5: e11046,
771 2010.
772
773 **Houser CR, Crawford GD, Barber RP, Salvaterra PM, and Vaughn JE**. Organization and
774 morphological characteristics of cholinergic neurons: an immunocytochemical study with a
775 monoclonal antibody to choline acetyltransferase. *Brain Res* 266: 97-119, 1983.

Huguenard JR, and Prince DA. A novel T-type current underlies prolonged Ca(2+)-dependent burst firing in GABAergic neurons of rat thalamic reticular nucleus. *J Neurosci* 12: 3804-3817, 1992.

Iijima K, and Kojima N. Gaba-T-positive neurons in the rat supraoptic nucleus as revealed by a pharmaco-histochemical method with gabaculine. *Acta Histochem Cytochem* 18: 445-454, 1985.

Iijima K, and Ogawa T. An HRP study on the distribution of all nuclei innervating the supraoptic nucleus in the rat brain. *Acta histochem* 69: 274-295, 1981.

Iijima K, Ohtomo K, Kobayashi R, and Kojima N. Immunohistochemical studies on the GABAergic system in the rat supraoptic nucleus using the PAP method with an application of electron microscopy. *Arch Histol Japon* 49: 579-591, 1986.

Iijima K, and Saito H. Histochemical studies on the distribution of thiamine pyrophosphatase and enzymes related to carbohydrate metabolism in the intercalated neurons of the rat supraoptic nucleus. *Am J Anat* 167: 265-273, 1983.

Israel JM, Poulain DA, and Oliet SH. Oxytocin-induced postinhibitory rebound firing facilitates bursting activity in oxytocin neurons. *J Neurosci* 28: 385-394, 2008.

Jhamandas JH, Raby W, Rogers J, Buijs RM, and Renaud LP. Diagonal band projection towards the hypothalamic supraoptic nucleus: light and electron microscopic observations in the rat. *J comp Neurol* 282: 15-23, 1989.

Karnani MM, Szábo G, Erdelyi F, and Burdakov D. Lateral hypothalamic GAD65 neurons are spontaneously firing and distinct from orexin- and melanin-concentrating hormone neurons. *J Physiol (Lond)* 591: 933-953, 2013.

Khateb A, Muhlethaler M, Alonso A, Serafin M, Mainville L, and Jones BE. Cholinergic nucleus basalis neurons display the capacity for rhythmic bursting activity mediated by low-threshold calcium spikes. *Neuroscience* 51: 489-494, 1992.

Kim U, and McCormick DA. The functional influence of burst and tonic firing mode on synaptic interactions in the thalamus. *J Neuroci:*18: 9500-9516, 1998.

Léranth C, Záborsky L, Marton J, and Palkovits M. Quantitative studies on the supraoptic nucleus in the rat. I. Synaptic organization. *Exp Brain Res* 22: 509-523, 1975.

Levine JD, Zhao XS, and Miselis RR. Direct and indirect retinohypothalamic projections to the supraoptic nucleus in the female albino rat. *J comp Neurol* 341: 214-224, 1994.

Lopez-Bendito G, Sturgess K, Erdelyi F, Szábo G, Molnar Z, and Paulsen O. Preferential origin and layer destination of GAD65-GFP cortical interneurons. *Cerebral Cortex* 14: 1122-1133, 2004.

LuQui IJ, and Fox CA. The supraoptic nucleus and supraopticohypophysial tract in the monkey (*Macaca mulatta*). *J comp Neurol* 168: 7-40, 1976.

826 **Luther JA, and Tasker JG**. Voltage-gated currents distinguish parvocellular from
827 magnocellular neurones in the rat hypothalamic paraventricular nucleus. *J Physiol (Lond)* 523:
828 193-209, 2000.
829
830 **Manns ID, Alonso A, and Jones BE.** Discharge properties of juxtacellularly labeled and
831 immunohistochemically identified cholinergic basal forebrain neurons recorded in association
832 with the electroencephalogram in anesthetized rats. *J Neurosci* 20: 1505-1518, 2000.
833
834 **Markram H, and Segal M**. Electrophysiological characteristics of cholinergic and non-
835 cholinergic neurons in the rat medial septum-diagonal band complex. *Brain Res* 513: 171-174,
836 1990.
837
838 **Mason WT, Ho YW, Eckenstein F, and Hatton GI**. Mapping of cholinergic neurons
839 associated with rat supraoptic nucleus: combined immunocytochemical and histochemical
840 identification. *Brain Res Bull* 11: 617-626, 1983.
841
842 **Meeker RB, Swanson DJ, and Hayward JN**. Local synaptic organization of cholinergic
843 neurons in the basolateral hypothalamus. *J. of comp neurol* 276: 157-168, 1988.
844
845 **Nagy PM, and Aubert I**. Overexpression of the vesicular acetylcholine transporter increased
846 acetylcholine release in the hippocampus. *Neuroscience* 218: 1-11, 2012.
847
848 **Nagy PM, and Aubert I**. B6eGFPChAT mice overexpressing the vesicular acetylcholine
849 transporter exhibit spontaneous hypoactivity and enhanced exploration in novel environments.
850 *Brain Behav* 3: 367-383, 2013.

Niespodziany I, Derambure P, and Poulain P. Properties of T-type calcium current in enkephalinergic neurones in guinea-pig hypothalamic slices. *Pflugers Archiv : Eur J Physiol* 437: 871-880, 1999.

Nissen R, Cunningham JT, and Renaud LP. Lateral hypothalamic lesions alter baroreceptor-evoked inhibition of rat supraoptic vasopressin neurones. *J Physiol (Lond)* 470: 751-766, 1993.

Okamura H, Abitbol M, Julien JF, Dumas S, Berod A, Geffard M, Kitahama K, Bobillier P, Mallet J, and Wiklund L. Neurons containing messenger RNA encoding glutamate decarboxylase in rat hypothalamus demonstrated by in situ hybridization, with special emphasis on cell groups in medial preoptic area, anterior hypothalamic area and dorsomedial hypothalamic nucleus. *Neuroscience* 39: 675-699, 1990.

Oliet SH, and Bourque CW. Properties of supraoptic magnocellular neurones isolated from the adult rat. *J Physiol (Lond)* 455: 291-306, 1992.

Mugnaini E, and Oertel WH. "An atlas of the distribution of GABAergic neurons and terminals in the rat CNS as revealed by GAD immunohistochemistry," in *Handbook of Chemical Neuroanatomy*, Vol. 4, *GABA and Neuropeptides in the CNS*, Part I, eds Bjorklund A., Hokfelt T., editors. (Amsterdam: Elsevier Science Publishers;), pp. 436–608, 1985.

Parrish-Aungst S, Shipley MT, Erdelyi F, Szábo G, and Puche AC. Quantitative analysis of neuronal diversity in the mouse olfactory bulb. *J comp Neurol* 501: 825-836, 2007.

Perez-Reyes E. Molecular physiology of low-voltage-activated t-type calcium channels. *Physiol Revs* 83: 117-161, 2003.

Raby WN, and Renaud LP. Dorsomedial medulla stimulation activates rat supraoptic oxytocin and vasopressin neurones through different pathways. *J Physiol (Lond)* 417: 279-294, 1989.

Randle J, Bourque CW, Renaud LP. Serial reconstruction of Lucifer yellow-labeled supraoptic nucleus neurons in perfused rat hypothalamic explants. *Neuroscience* 17: 453-467, 1986.

Rao ZR, Yamano M, Wanaka A, Tatehata T, Shiosaka S, and Tohyama M. Distribution of cholinergic neurons and fibers in the hypothalamus of the rat using choline acetyltransferase as a marker. *Neuroscience* 20: 923-934, 1987.

Rodriguez-Sierra JF, and Morley BJ. Evidence that cell bodies in the arcuate nucleus of the hypothalamus are not cholinergic. *Neuroendocr* 41: 427-431, 1985.

Roland BL, and Sawchenko PE. Local origins of some GABAergic projections to the paraventricular and supraoptic nuclei of the hypothalamus in the rat. *J Comp Neurol* 332: 123-143, 1993.

Shin SY, Yang JH, Lee H, Erdelyi F, Szábo G, Lee SY, and Ryu PD. Identification of the adrenoceptor subtypes expressed on GABAergic neurons in the anterior hypothalamic area and rostral zona incerta of GAD65-eGFP transgenic mice. *Neurosci Lett* 422: 153-157, 2007.

Shin SY, Han TH, Lee SY, Han SK, Park JB, Erdelyi F, Szábo G, and Ryu PD. Direct Corticosteroid Modulation of GABAergic Neurons in the Anterior Hypothalamic Area of GAD65-eGFP Mice. *Korean J Physiol Pharmacol* 15: 163-169, 2011.

Sladek CD, and Joynt RJ. Characterization of cholinergic control of vasopressin release by the organ-cultured rat hypothalamo-neurohypophyseal system. *Endocrinology* 104: 659-663, 1979a.

Sladek CD, and Joynt RJ. Cholinergic involvement in osmotic control of vasopressin release by the organ-cultured rat hypothalamo-neurohypophyseal system. *Endocrinology* 105: 367-371, 1979b.

Smith BN, and Armstrong WE. Tuberal supraoptic neurons--I. Morphological and electrophysiological characteristics observed with intracellular recording and biocytin filling in vitro. *Neuroscience* 38: 469-483, 1990.

Starostik MR, Rebello MR, Cotter KA, Kulik A, and Medler KF. Expression of GABAergic receptors in mouse taste receptor cells. *PloS one* 5: e13639, 2010.

Stern JE. Electrophysiological and morphological properties of pre-autonomic neurones in the rat hypothalamic paraventricular nucleus. *J Physiol (Lond)* 537: 161-177, 2001.

Stern JE, and Armstrong WE. Changes in the electrical properties of supraoptic nucleus oxytocin and vasopressin neurons during lactation. *J Neurosci* 16: 4861-4871, 1996.

Stern JE, and Armstrong WE. Reorganization of the dendritic trees of oxytocin and vasopressin neurons of the rat supraoptic nucleus during lactation. *J Neurosci* 18: 841-853, 1998.

Tago H, McGeer PL, Bruce G, and Hersh LB. Distribution of choline acetyltransferase-containing neurons of the hypothalamus. *Brain Res* 415: 49-62, 1987.

Tallini YN, Shui B, Greene KS, Deng KY, Doran R, Fisher PJ, Zipfel W, and Kotlikoff MI. BAC transgenic mice express enhanced green fluorescent protein in central and peripheral cholinergic neurons. *Physiol Genomics* 27: 391-397, 2006.

Tappaz ML, Wassef M, Oertel WH, Paut L, and Pujol JF. Light and electronmicroscopic immunocytochemistry of glutamic acid decarboxylase (GAD) in the basal hypothalamus: Morphological evidence for neuroendocrine γ-aminobutyrate (GABA). *Neuroscience* 9: 271-287,
1983.

Tasker JG, and Dudek FE. Electrophysiological properties of neurones in the region of the paraventricular nucleus in slices of rat hypothalamus. *J Physiol (Lond)* 434: 271-293, 1991.

Teruyama R, and Armstrong WE. Enhancement of calcium-dependent afterpotentials in oxytocin neurons of the rat supraoptic nucleus during lactation. *J Physiol* 566: 505-518, 2005.

Teruyama R, Sakuraba M, Wilson LL, Wandrey NE, and Armstrong WE. Epithelial Na(+) sodium channels in magnocellular cells of the rat supraoptic and paraventricular nuclei. *Am J Physiol Endocrinol Metab* 302: E273-285, 2012.

951

952 **Theodosis DT, and Mason WT**. Choline acetyltransferase immunocytochemical staining of the
953 rat supraoptic nucleus and its surroundings. A light- and electron-microscopic study. *Cell Tiss*
954 *Res* 254: 119-124, 1988.

955

956 **Theodosis DT, Paut L, and Tappaz ML.** Immunocytochemical analysis of the GABAergic
957 innervation of oxytocin- and vasopressin-secreting neurons in the rat supraoptic nucleus.
958 *Neuroscience* 19: 207-222, 1986.

959

960 **Tribollet E, Armstrong WE, Dubois-Dauphin M, and Dreifuss J-J**. Extrahypothalamic
961 afferent inputs to the supraoptic nucleus area of the rat as determined by retrograde and
962 anterograde tracing techniques. *Neuroscience* 15: 135-148, 1985.

963

964 **Wierenga CJ, Mullner FE, Rinke I, Keck T, Stein V, and Bonhoeffer T**. Molecular and
965 electrophysiological characterization of GFP-expressing CA1 interneurons in GAD65-GFP mice.
966 *PloS one* 5: e15915, 2010.

967

968 **Woolf NJ, Eckenstein F, and Butcher LL**. Cholinergic projections from the basal forebrain to
969 the frontal cortex: a combined fluorescent tracer and immunohistochemical analysis in the rat.
970 *Neurosci Lett* 40: 93-98, 1983.

971

972 **Wuarin JP**. Glutamate microstimulation of local inhibitory circuits in the supraoptic nucleus
973 from rat hypothalamus slices. *J Neurophysiol* 78: 3180-3186, 1997.

974

Zaninetti M, Tribollet E, Bertrand D, and Raggenbass M. Nicotinic cholinergic activation of magnocellular neurons of the hypothalamic paraventricular nucleus. *Neuroscience* 110: 287-299, 2002.

Zhang C, Szábo G, Erdelyi F, Rose JD, and Sun QQ. Novel interneuronal network in the mouse posterior piriform cortex. *J comp Neurol* 499: 1000-1015, 2006.

Figure Legends

Figure 1. *Confocal image of GAD65-eGFP PNZ neurons near the SON.* Distribution of GAD65 eGFP neurons near the SON in coronal sections of mouse hypothalamus. **A**: Confocal projection image (9, 0.85 μm optical sections) from a stack through one side of the SON stained for vasopressin-neurophysin to highlight VP neurons (red). Numerous GAD-eGFP neurons (green) are evident in the PNZ, and lie close to, but only rarely among, SON neurons. OpT, optic tract. **B**: As in **A**, but in a more rostral section from the same mouse stained for oxytocin-neurophysin to highlight OT neurons (10, 0.86 μm optical sections). OpC, optic chiasm.

Figure 2. *Confocal image of GAD65-eGFP PNZ neurons near the PVN.* Confocal projection image from a stack through the PVN (9, 0.86 μm optical sections), also stained for vasopressin-neurophysin (red) to show PVN boundaries. Numerous GAD65-eGFP neurons are visible in the anterior hypothalamus ventro-lateral to the PVN, in the zona incerta (ZI), and some very near the PVN (arrows). 3V, third ventricle; Re, thalamic reuniens nucleus.

Figure 3. *Electrophysiological characteristics of GAD65-eGFP PNZ neurons.* **A** and **B**: Responses of a PNZ neuron to current injection (400 ms) at 2 different membrane potentials. **A**: When the membrane potential was hyperpolarized, depolarizing pulses first evoked an LTS (vertical arrow), and slightly stronger pulses evoked a brief burst of fast spikes on top of the LTS. **B**: When the membrane potential was held at –57 mV (just below the threshold of spontaneous firing), a rebound LTS (vertical arrow) was similarly evoked following release of a hyperpolarizing pulse. Hyperpolarizing pulses also revealed inward rectification (horizontal arrow) characteristic of neurons with I_h. These characteristics were similar to those of most unlabeled, small PNZ neurons as well as those previously reported from this lab (Armstrong and

Stern, 1997).

Figure 4. *The LTS is not blocked by $NiCl_2$ or TTX.* **A:** A GAD65-eGFP PNZ neuron exhibiting LTS (arrow) to depolarizing current. Note that the fast spikes arising from the LTS are clipped. **B**: 100 μM $NiCl_2$ was applied, and the LTS (arrow) was little affected, whereas the trace noise (presumptively synaptic) was reduced. Fast spikes are clipped as in **A**. Baseline, -90 mV. **C**: Responses of another GAD65 PNZ neuron to depolarizing current injection (400 ms). Depolarizing pulses evoked an LTS (arrow), the strongest of which led to a fast Na^+ spike. **D**: In the presence of 500 nM TTX, the fast spike is blocked and the full expression of an LTS is visible (arrow). **E**: The slice was then exposed to 100 μM $NiCl_2$, which failed to suppress the LTS (arrow). Horizontal line shows the peak of the LTS in TTX.

Figure 5. *Spontaneous firing patterns of GAD65-eGFP neurons.* On the left are sample records extracted from longer recordings, on the right are interspike interval (ISI) histograms from 1-2 min of activity. **A**: A relatively fast (12.7 $\pm$ 1 Hz; $\bar{x}$ ± s.d.), continuously firing neuron with a regular interspike interval (CV = 0.07) and a normally distributed ISI. **B**: A relatively slow (5.7 $\pm$ 1.7 Hz; $\bar{x}$ ± s.d.),), irregularly firing neuron (CV = 0.48) showing a Poisson ISI distribution. **C:** A bursting neuron. Excluding the 7 outlying ISIs of the long (> 1 sec) interburst intervals, the intraburst firing rate was 4.9 ± 1.4 Hz, the intraburst CV = 0.45 and ISI distribution were similar to the cell in **B**.

Figure 6. *Filled GAD65-eGFP neurons in the PNZ.* **A**: Photomicrograph of biocytin-filled neuron in coronal section taken from a Z stack of 9, 1.5 μm steps. The rostral part of the SON and optic chiasm (OpC) are medial, to the left. All processes were relatively thin and it was not possible to discern an axon from dendrites. The soma lay just lateral to the SON and one

1037 branching process projected over the SON. The reconstruction is shown just below, in **C**. **B**:
1038 Another projection from a filled neuron taken from a Z stack of 15, 1 μm steps and its
1039 reconstruction (**D**). This neuron lay dorsal to the SON, caudal to the neuron shown in **A**, and the
1040 processes projecting ventrolaterally encroached on the SON, whereas as a medial process
1041 projected over the nucleus. As with the neuron shown in **A**, it was difficult to distinguish an axon
1042 from the other processes. Bar = 100 μm in all frames. Opt, optic tract.
1043
1044 **Figure 7.** *Confocal image of ChAT-eGFP neurons near the SON in coronal sections of mouse*
1045 *hypothalamus*. **A**: Confocal projection from a stack through one side of the SON stained for
1046 vasopressin-neurophysin to highlight VP neurons (red) (14, 0.95 μm optical sections).
1047 Numerous large ChAT-eGFP neurons (double arrows, green neurons) are evident and lie close
1048 to, but not among, SON neurons. Weakly fluorescent, smaller neurons are also visible (arrow).
1049 **B**: Another projection stack through a different section from the same ChAT-eGFP mouse,
1050 stained for oxytocin-neurophysin (red) (14, 1.05 μm optical sections). Some of the bright, larger
1051 ChAT-eGFP neurons (green) lay close to the SON, with processes extending into the dorsal part
1052 of the nucleus in the case of the neuron on the lower left. Note in both the presence of more
1053 weakly fluorescent green eGFP neurons, some of which are found very close to, even within, the
1054 SON (arrows). OpT, optic tract.
1055
1056 **Figure 8.** *Anti-ChAT antibody labels large, but not small ChAT-eGFP neurons near the SON.* **A**:
1057 Confocal projection image from a stack through one side of the SON (arrow) stained for ChAT
1058 (red neurons) (10, 0.86 μm optical sections). Numerous large ChAT-positive neurons are
1059 evident, two of which are indicated by double arrows. Single arrow points to location of the
1060 SON. **B**: the same section as in **A**, showing ChAT-eGFP neurons. Note the small, weakly
1061 fluorescent eGFP neurons near the SON (arrow), and a smaller but brightly fluorescent eGFP

neuron (arrowhead). **C**: overlap of **A** and **B** showing that only large, brighter ChAT-eGFP neurons stain positive with the anti-ChAT ab. Note the one bright, small eGFP neuron did not stain for anti-ChAT (arrowhead**).** OpT, optic tract.

Figure 9. *Electrophysiological characteristics of ChAT-eGFP PNZ neurons.* **A** and **C**: Responses of a large ChAT-eGFP neuron to current injection at 2 different membrane potentials. **A**: When the membrane potential was held hyperpolarized, depolarizing pulses (800 ms) evoked a transient outward rectification (arrow), with a depolarizing ramp leading to an action potential at the most depolarized current injection. Note also that subthreshold to the fast spike, a small, delayed depolarizing bump was also observed (double arrows; gray trace) **C**: When the membrane potential was held at –48 mV (just below the threshold of spontaneous firing), a similar outward rectification (arrow) was seen following the offset of hyperpolarizing pulses (400 ms). These hyperpolarizing pulses also revealed some slow inward rectification (*) characteristic of neurons with I_h. Note also the large spike HAP (double arrow). **B and D**: Responses of a smaller, weakly fluorescent ChAT-eGFP neuron to protocols identical to those in **A** and **C**. **B**: When the membrane potential was held at –83 mV, the largest depolarizing pulse evoked an LTS with a pair of fast spikes (arrow). **D**: When the membrane potential was held at –67 mV, a rebound LTS (arrows) that in one trace leads to a fast spike (upper arrow) was similarly evoked following release of a hyperpolarizing pulse. Hyperpolarizing pulses also revealed inward rectification (*) characteristic of neurons with I_h. These characteristics were similar to those of the smaller neurons recorded in the GAD65-eGFP mice (see Fig. 3).

Figure 10. *Filled ChAT-eGFP neurons in the PNZ.* **A**: Photomicrograph of biocytin-filled large neuron in coronal section with a polygonal soma, projected from a Z stack of 18, 2.7 µm steps. The rostral part of the SON and optic chiasm (OpC) are to the right. The soma lay dorso-lateral

to the SON. One thin process projects toward the SON, but is cut at the slice surface as indicated by the retraction ball (arrow)- this is likely an axon. **B**: The reconstruction of cell shown in **A**. **C**: Three small ChAT-eGFP neuron reconstructions. Note the difference in soma size compared to the large neuron. All three are oriented in the coronal slice similar to neuron shown in **A**, but each neuron was found dorsal to the SON and had processes with a limited extent within the slice, characteristic of most small ChAT-eGFP neurons. In each case, retraction balls are present (arrows)-there are two such balls from branching processes in cells 1 and 3. **D.** Photomicrograph of biocytin-filled large neuron with a rounded soma and a vertical orientation, projected from a Z stack of 15, 2.7 μm steps. This neuron had an axon with a fairly extensive collateral arbor, visible in the reconstruction in **E** (arrows). Bars = 100 μm.

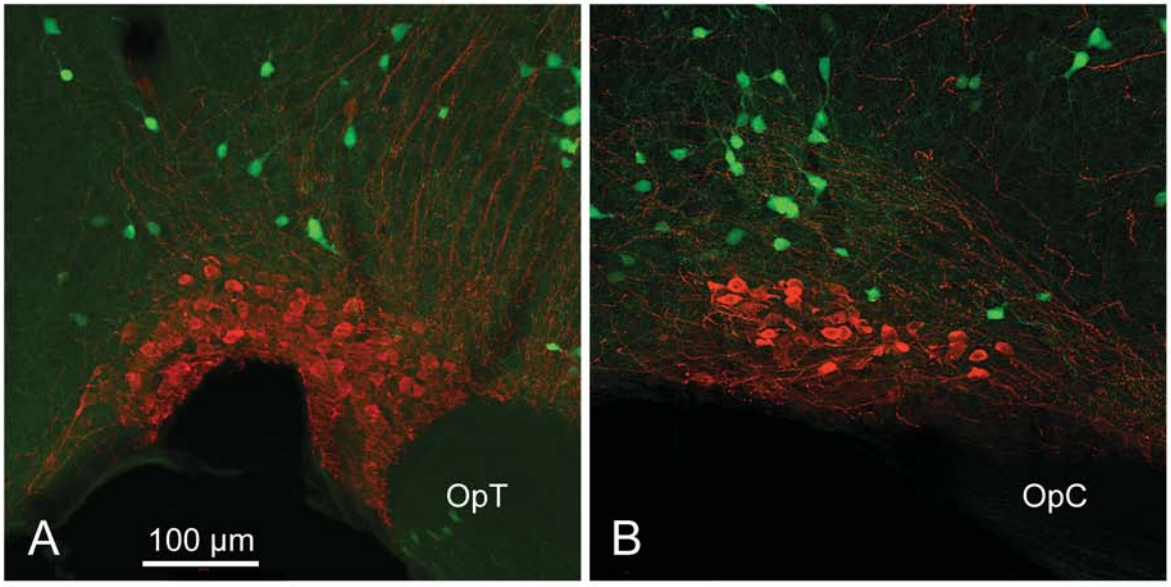

Figure 1. Confocal image of GAD65-eGFP PNZ neurons near the SON. Distribution of GAD65 eGFP neurons near the SON in coronal sections of mouse hypothalamus. **A**: Confocal projection image (9, 0.85 μm optical sections) from a stack through one side of the SON stained for vasopressin-neurophysin to highlight VP neurons (red). Numerous GAD-eGFP neurons (green) are evident in the PNZ, and lie close to, but only rarely among, SON neurons. OpT, optic tract. **B**: As in **A**, but in a more rostral section from the same mouse stained for oxytocin-neurophysin to highlight OT neurons (10, 0.86 μm optical sections). OpC, optic chiasm.

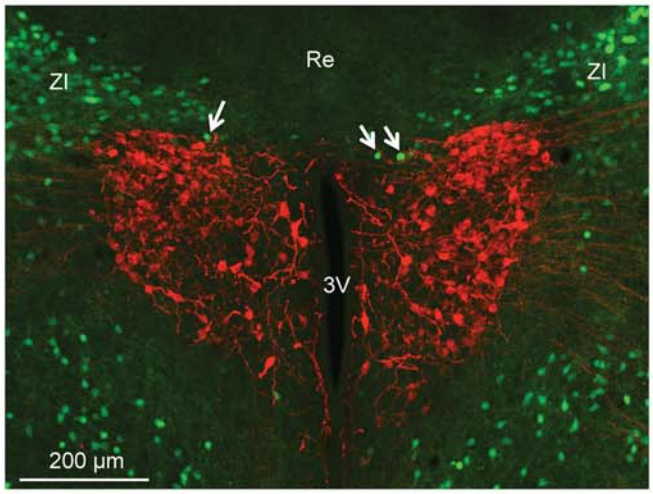

Figure 2. Confocal image of GAD65-eGFP PNZ neurons near the PVN. Confocal projection image from a stack through the PVN (9, 0.86 μm optical sections), also stained for vasopressin-neurophysin (red) to show PVN boundaries. Numerous GAD65-eGFP neurons are visible in the anterior hypothalamus ventro-lateral to the PVN, in the zona incerta (ZI), and some very near the PVN (arrows). 3V, third ventricle; Re, thalamic reuniens nucleus.

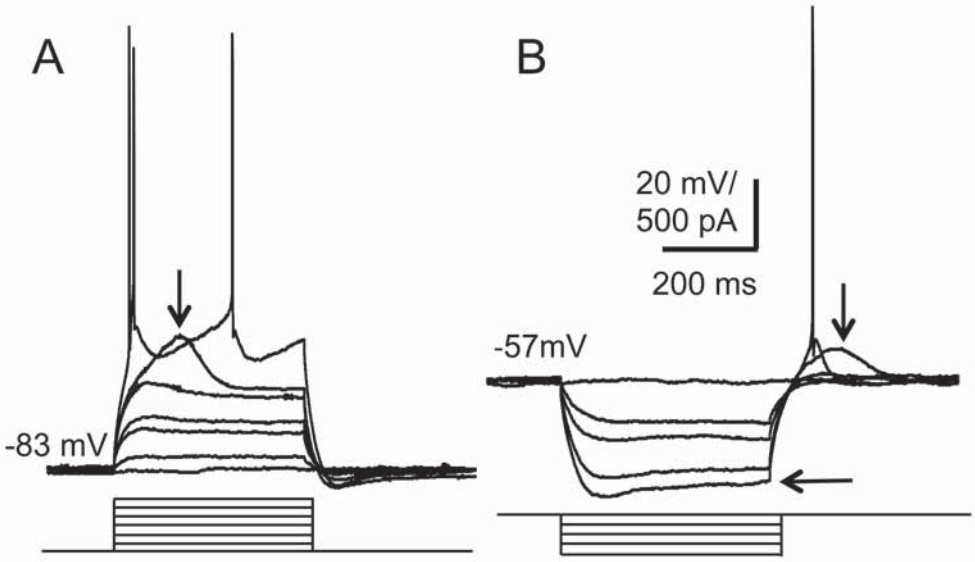

Figure 3. Electrophysiological characteristics of GAD65-eGFP PNZ neurons. **A** and **B**: Responses of a PNZ neuron to current injection (400 ms) at 2 different membrane potentials. **A**: When the membrane potential was hyperpolarized, depolarizing pulses first evoked an LTS (vertical arrow), and slightly stronger pulses evoked a brief burst of fast spikes on top of the LTS. **B**: When the membrane potential was held at –57 mV (just below the threshold of spontaneous firing), a rebound LTS (vertical arrow) was similarly evoked following release of a hyperpolarizing pulse. Hyperpolarizing pulses also revealed inward rectification (horizontal arrow) characteristic of neurons with Ih. These characteristics were similar to those of most unlabeled, small PNZ neurons as well as those previously reported from this lab (Armstrong and Stern, 1997).

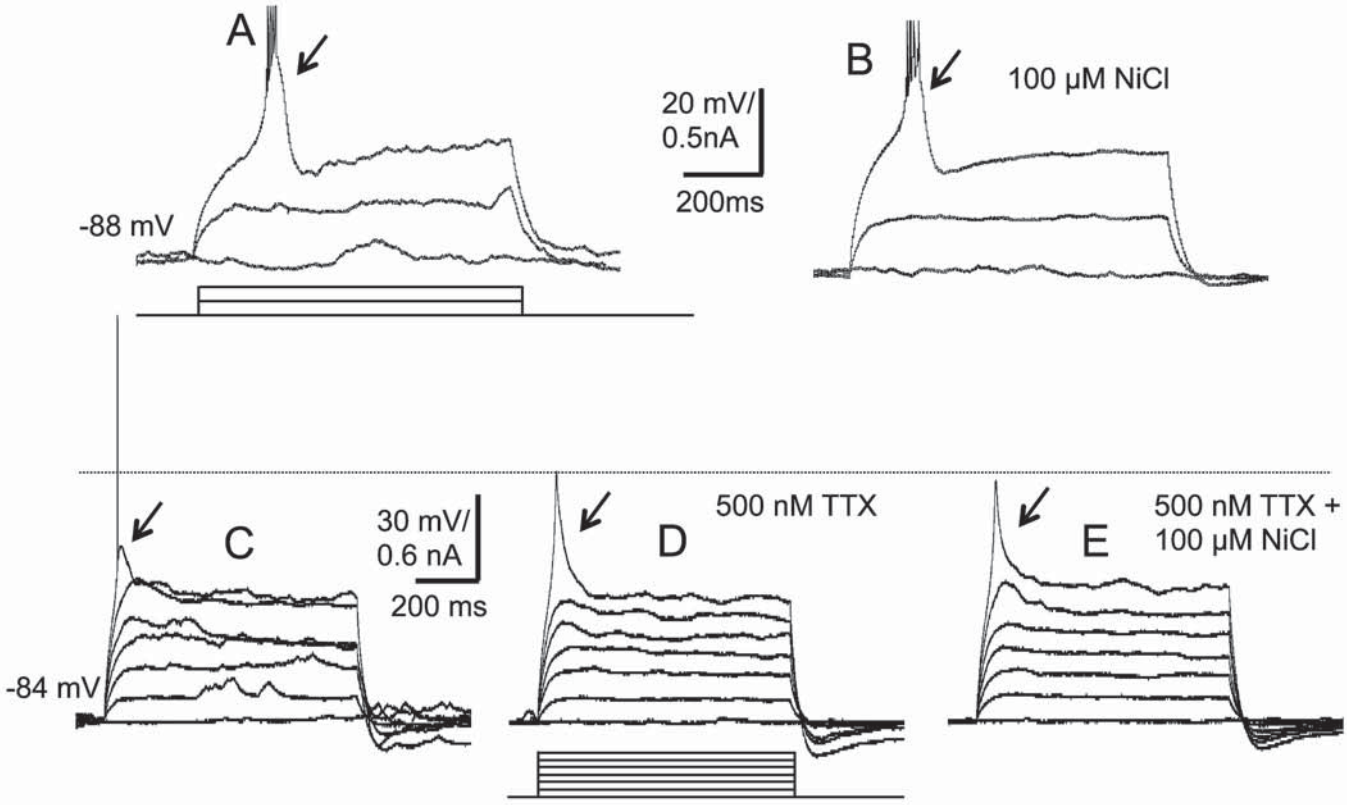

Figure 4. The LTS is not blocked by NiCl2 or TTX. **A**: A GAD65-eGFP PNZ neuron exhibiting LTS (arrow) to depolarizing current. Note that the fast spikes arising from the LTS are clipped. **B**: 100 μM NiCl2 was applied, and the LTS (arrow) was little affected, whereas the trace noise (presumptively synaptic) was reduced. Fast spikes are clipped as in **A**. Baseline, -90 mV. **C**: Responses of another GAD65 PNZ neuron to depolarizing current injection (400 ms). Depolarizing pulses evoked an LTS (arrow), the strongest of which led to a fast Na+ spike. **D**: In the presence of 500 nM TTX, the fast spike is blocked and the full expression of an LTS is visible (arrow). **E**: The slice was then exposed to 100 μM NiCl2, which failed to suppress the LTS (arrow). Horizontal line shows the peak of the LTS in TTX.

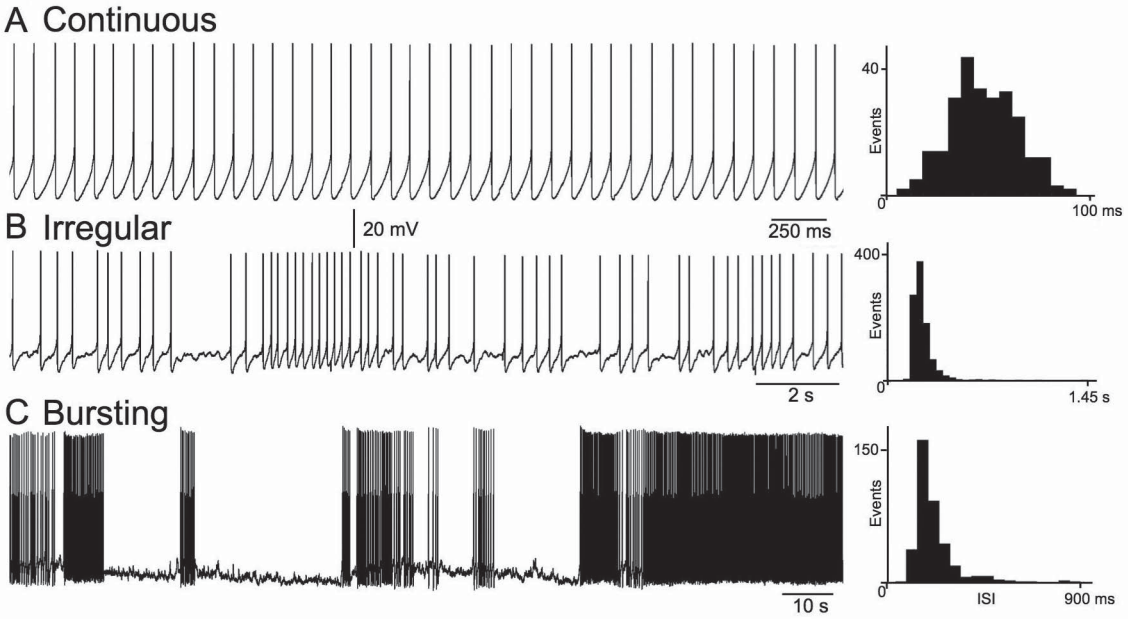

Figure 5. Spontaneous firing patterns of GAD65-eGFP neurons. On the left are sample records extracted from longer recordings, on the right are interspike interval (ISI) histograms from 1-2 min of activity. **A**: A relatively fast (12.7 + 1 Hz; x ± s.d.), continuously firing neuron with a regular interspike interval (CV = 0.07) and a normally distributed ISI. **B**: A relatively slow (5.7 + 1.7 Hz; x ± s.d.),), irregularly firing neuron (CV = 0.48) showing a Poisson ISI distribution. **C**: A bursting neuron. Excluding the 7 outlying ISIs of the long (> 1 sec) interburst intervals, the intraburst firing rate was 4.9 ± 1.4 Hz, the intraburst CV = 0.45 and ISI distribution were similar to the cell in **B**.

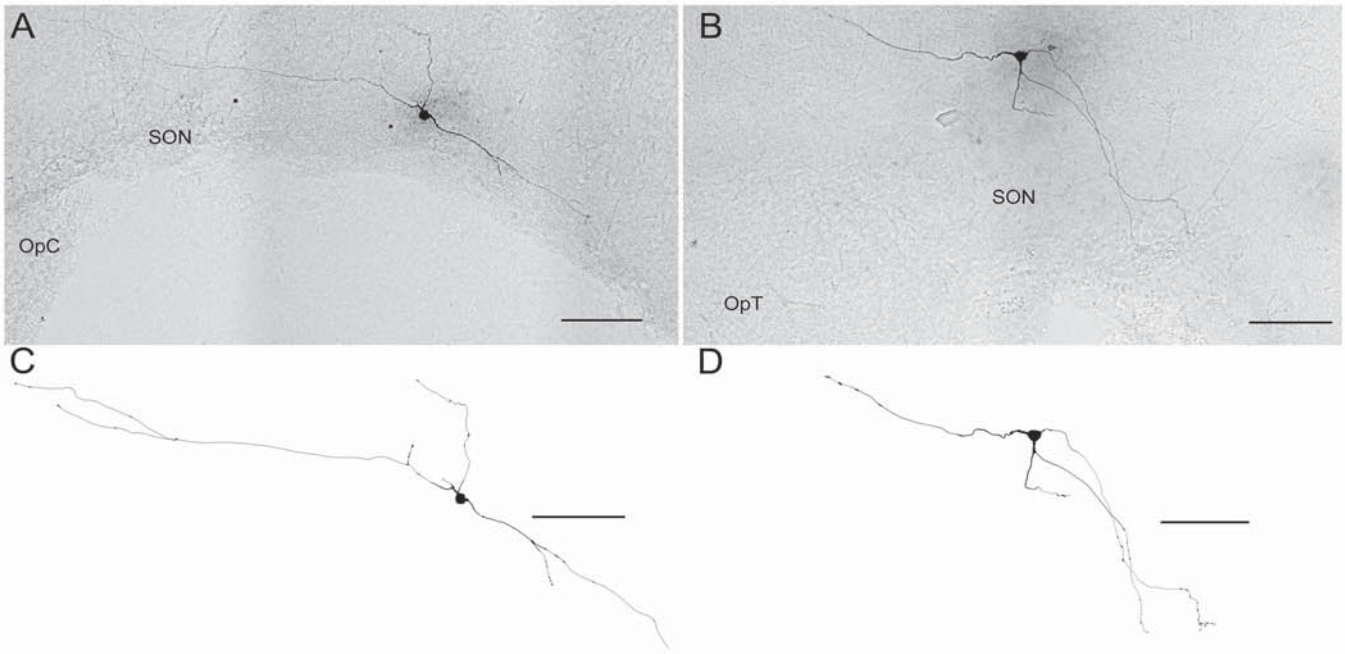

Figure 6. Filled GAD65-eGFP neurons in the PNZ. **A**: Photomicrograph of biocytin-filled neuron in coronal section taken from a Z stack of 9, 1.5 μm steps. The rostral part of the SON and optic chiasm (OpC) are medial, to the left. All processes were relatively thin and it was not possible to discern an axon from dendrites. The soma lay just lateral to the SON and one branching process projected over the SON. The reconstruction is shown just below, in **C**. **B**: Another projection from a filled neuron taken from a Z stack of 15, 1 μm steps and its reconstruction (**D**). This neuron lay dorsal to the SON, caudal to the neuron shown in A, and the processes projecting ventrolaterally encroached on the SON, whereas as a medial process projected over the nucleus. As with the neuron shown in **A**, it was difficult to distinguish an axon from the other processes. Bar = 100 μm in all frames. Opt, optic tract.

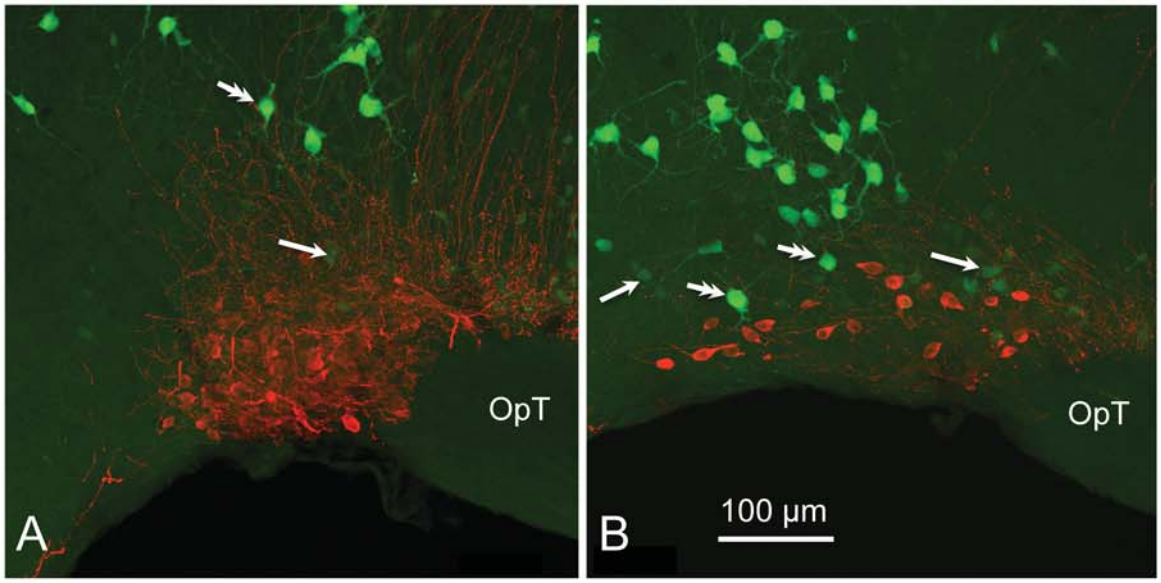

Figure 7. Confocal image of ChAT-eGFP neurons near the SON in coronal sections of mouse hypothalamus. **A**: Confocal projection from a stack through one side of the SON stained for vasopressin-neurophysin to highlight VP neurons (red) (14, 0.95 μm optical sections). Numerous large ChAT-eGFP neurons (double arrows, green neurons) are evident and lie close to, but not among, SON neurons. Weakly fluorescent, smaller neurons are also visible (arrow). **B**: Another projection stack through a different section from the same ChAT-eGFP mouse, stained for oxytocin-neurophysin (red) (14, 1.05 μm optical sections). Some of the bright, larger ChAT-eGFP neurons (green) lay close to the SON, with processes extending into the dorsal part of the nucleus in the case of the neuron on the lower left. Note in both the presence of more weakly fluorescent green eGFP neurons, some of which are found very close to, even within, the SON (arrows). OpT, optic tract.

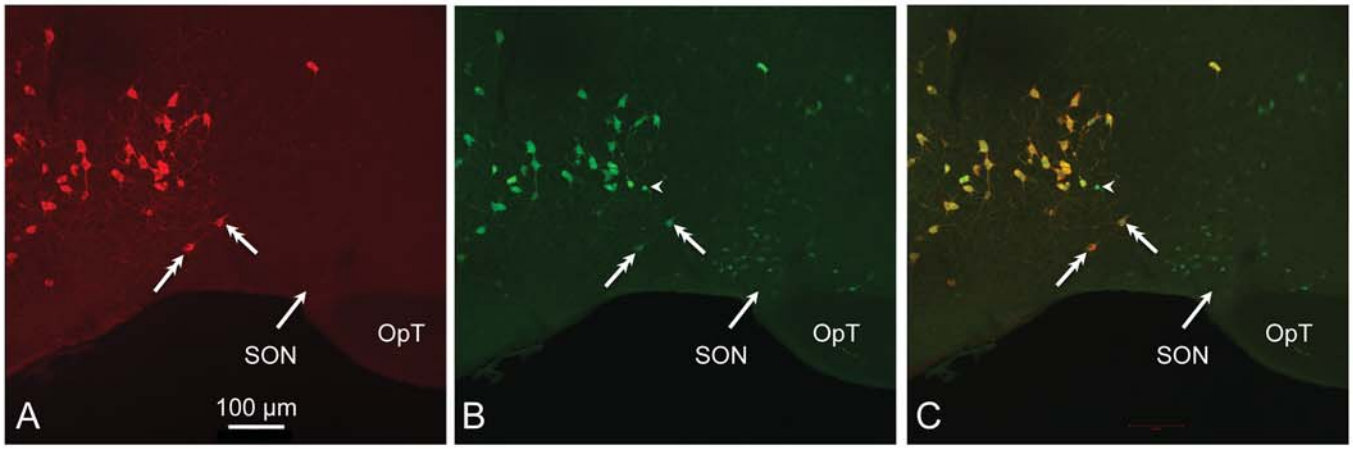

Figure 8. Anti-ChAT antibody labels large, but not small ChAT-eGFP neurons near the SON. **A**: Confocal projection image from a stack through one side of the SON (arrow) stained for ChAT (red neurons) (10, 0.86 μm optical sections). Numerous large ChAT-positive neurons are evident, two of which are indicated by double arrows. Single arrow points to location of the SON. **B**: the same section as in A, showing ChAT-eGFP neurons. Note the small, weakly fluorescent eGFP neurons near the SON (arrow), and a smaller but brightly fluorescent eGFP neuron (arrowhead). **C**: overlap of **A** and **B** showing that only large, brighter ChAT-eGFP neurons stain positive with the anti-ChAT ab. Note the one bright, small eGFP neuron did not stain for anti-ChAT (arrowhead). OpT, optic tract.

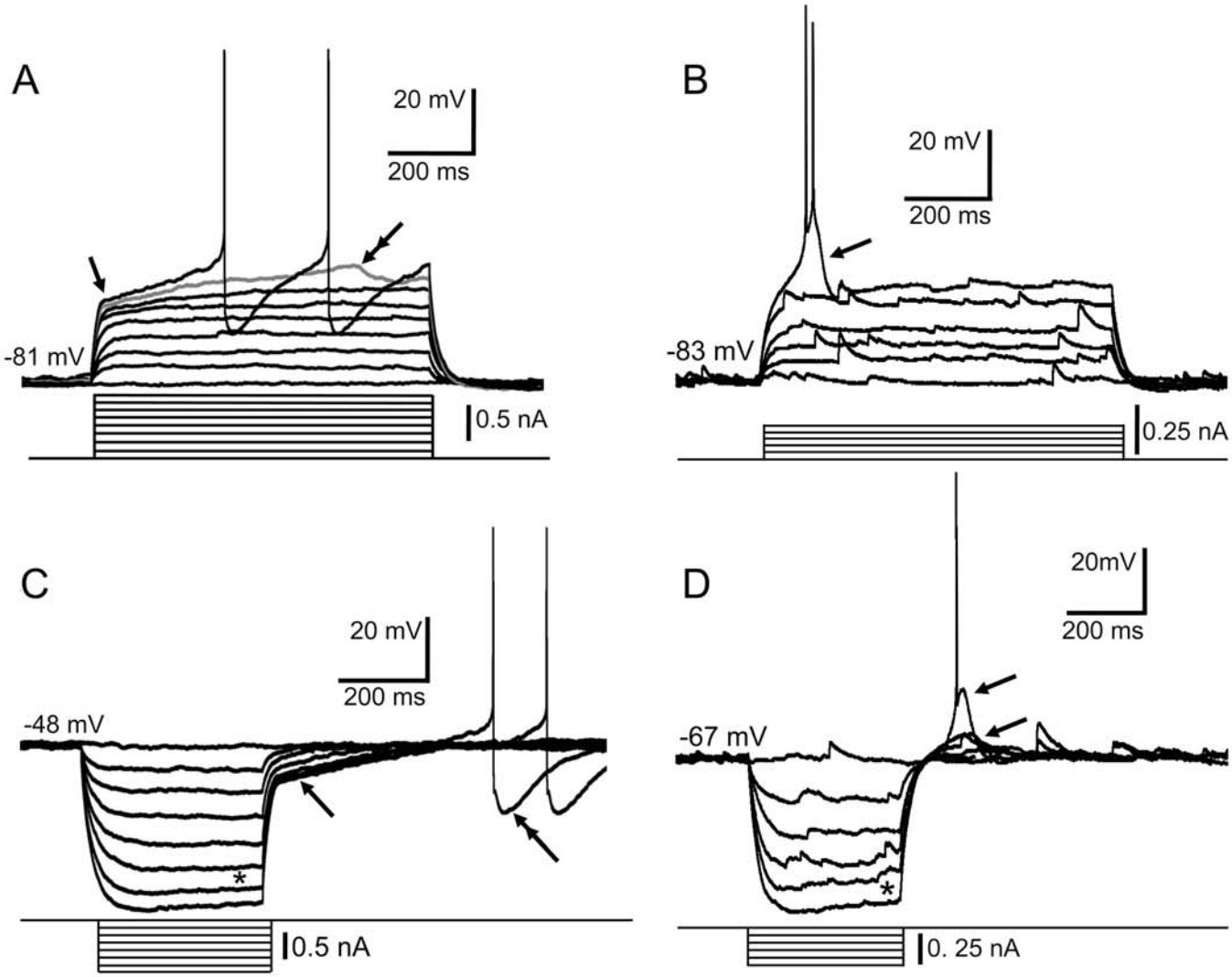

Figure 9. Electrophysiological characteristics of ChAT-eGFP PNZ neurons. **A** and **C**: Responses of a large ChAT-eGFP neuron to current injection at 2 different membrane potentials. **A**: When the membrane potential was held hyperpolarized, depolarizing pulses (800 ms) evoked a transient outward rectification (arrow), with a depolarizing ramp leading to an action potential at the most depolarized current injection. Note also that subthreshold to the fast spike, a small, delayed depolarizing bump was also observed (double arrows; gray trace) **C**: When the membrane potential was held at –48 mV (just below the threshold of spontaneous firing), a similar outward rectification (arrow) was seen following the offset of hyperpolarizing pulses (400 ms). These hyperpolarizing pulses also revealed some slow inward rectification (*) characteristic of neurons with Ih. Note also the large spike HAP (double arrow). **B** and **D**: Responses of a smaller, weakly fluorescent ChAT-eGFP neuron to protocols identical to those in **A** and **C**. **B**: When the membrane potential was held at –83 mV, the largest depolarizing pulse evoked an LTS with a pair of fast spikes (arrow). **D**: When the membrane potential was held at –67 mV, a rebound LTS (arrows) that in one trace leads to a fast spike (upper arrow) was similarly evoked following release of a hyperpolarizing pulse. Hyperpolarizing pulses also revealed inward rectification (*) characteristic of neurons with Ih. These characteristics were similar to those of the smaller neurons recorded in the GAD65-eGFP mice (see Fig. 3).

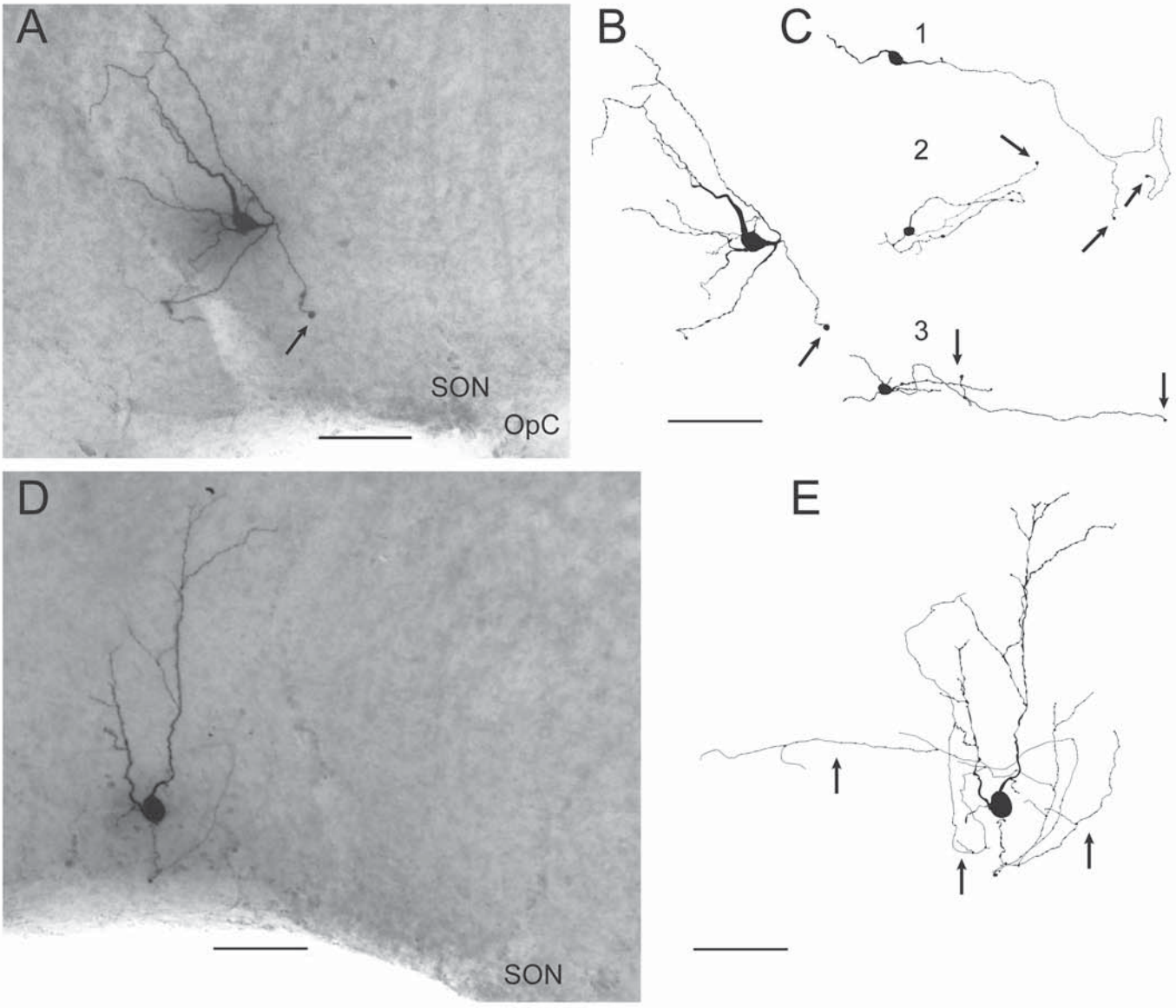

Figure 10. Filled ChAT-eGFP neurons in the PNZ. **A**: Photomicrograph of biocytin-filled large neuron in coronal section with a polygonal soma, projected from a Z stack of 18, 2.7 μm steps. The rostral part of the SON and optic chiasm (OpC) are to the right. The soma lay dorso-lateral to the SON. One thin process projects toward the SON, but is cut at the slice surface as indicated by the retraction ball (arrow)- this is likely an axon. **B**: The reconstruction of cell shown in **A**. **C**: Three small ChAT-eGFP neuron reconstructions. Note the difference in soma size compared to the large neuron. All three are oriented in the coronal slice similar to neuron shown in **A**, but each neuron was found dorsal to the SON and had processes with a limited extent within the slice, characteristic of most small ChAT-eGFP neurons. In each case, retraction balls are present (arrows)-there are two such balls from branching processes in cells 1 and 3. **D**. Photomicrograph of biocytin-filled large neuron with a rounded soma and a vertical orientation, projected from a Z stack of 15, 2.7 μm steps. This neuron had an axon with a fairly extensive collateral arbor, visible in the reconstruction in **E** (arrows). Bars = 100 µm.